Article

Rh(DPEPhos)-Catalyzed Alkyne Hydroacylation using #-Carbonyl Substituted Aldehydes. Mechanistic Insight Leads to Low Catalyst Loadings that Enables Selective Catalysis on Gram-Scale.

James Barwick-Silk, Simon Hardy, Michael C. Willis, and Andrew S. Weller

J. Am. Chem. Soc., **Just Accepted Manuscript** • DOI: 10.1021/jacs.8b04086 • Publication Date (Web): 15 May 2018

Rh(DPEPhos)-Catalyzed Alkyne Hydroacylation using β-Carbonyl Substituted Aldehydes. Mechanistic Insight Leads to Low Catalyst Loadings that Enables Selective Catalysis on Gram-Scale.

James Barwick-Silk[†], Simon Hardy[‡], Michael C. Willis[†] and Andrew S. Weller[†*]

†Department of Chemistry, Chemistry Research Laboratories, University of Oxford, Mansfield Road, OX1 4TA, U.K;
‡Early Chemical Development, Pharmaceutical Sciences, IMED Biotech Unit, AstraZeneca, Macclesfield, UK, SK10 2NA, U.K.

ABSTRACT: The detailed mechanism of the hydroacylation of *β*-amido–aldehyde, 2,2-dimethyl-3-morpholino-3-oxopropanal, with 1–octyne using [Rh(*cis*-κ^2-$_{P,P}$-DPEPhos)(acetone)$_2$][BAr$^F_4$]–based catalysts is described [Ar^F = (CF$_3$)$_2$C$_6$H$_3$]. A rich mechanistic landscape of competing and interconnected hydroacylation and cyclotrimerization processes is revealed. An acyl-hydride complex, arising from oxidative addition of aldehyde, is the persistent resting state during hydroacylation, and quaternary substitution at the *β*-amido–aldehyde strongly disfavours decarbonylation. Initial rate, KIE and labelling studies suggest that the migratory insertion is turnover-limiting as well as selectivity determining (linear/branched products). When the concentration of free aldehyde approaches zero at the later stages of catalysis alkyne cyclotrimerization becomes competitive, to form tri–substituted hexylarenes. At this point the remaining acyl hydride turns over in hydroacylation and the free alkyne is now effectively in excess, and the resting state moves to a metallacyclopentadiene and eventually to a dormant α–pyran–bound catalyst complex. Cyclotrimerization thus only becomes competitive when there is no aldehyde present in solution, and as aldehyde binds so strongly to form acyl-hydride when this happens will directly correlate to catalyst loading: with low loadings allowing for free aldehyde to be present for longer, and thus higher selectivites to be obtained. Reducing the catalyst loading from 20 mol% to 0.5 mol% thus leads to a selectivity increase from 96% to ~100%. An optimized hydroacylation reaction is described that delivers gram scale of product, at essentially quantitative levels, using no excess of either reagent, at very low catalyst loadings, using minimal solvent, with virtually no workup.

1. Introduction. Hydroacylation (HA) is a C–C bond forming reaction between an aldehyde and an alkyne or alkene to form an enone or ketone respectively (Scheme 1A), via an atom efficient, sequential, C–H activation and C–C coupling.[1-2] The development of intermolecular hydroacylation is particularly attractive, due to the availability of an enormous variety of potential coupling partners. Although significant focus has been placed upon methodologies using non-tethered aldehydes, promoted by Ru,[3-7] Ni,[8-9] Co[10-11] and Rh-based catalysts,[12-18] systems that provide the broadest substrate scope utilise tethered-aldehydes, including, PR_2,[19] alkene,[20] NR_2,[21-22] OH[23-27] and SR groups,[28-32] in combination with Rh-chelated phosphine catalysts (Scheme 1B). The generally proposed mechanism for these reactions involves oxidative addition of the aldehyde to give an acyl-hydride, followed by co-ordination and migratory insertion of the alkyne/alkene, and finally reductive elimination to form the enone/ketone (Scheme 1C).[33-34] A competitive process to productive hydroacylation occurs by bifurcation of the reaction pathway at the acyl-hydride intermediate. This intermediate can undergo reversible decarbonylation, followed by irreversible reductive elimination to form a Rh-carbonyl complex and an alkane (Scheme 1C). Attenuating this process is central to the delivery of robust, scalable and broadly applicable catalyst systems, as this side-reaction can cause irreversible catalyst deactivation.[13,35-39]

As well as the identity of the aldehyde and olefin playing a significant role in promoting productive hydroacylation over reductive decarbonylation,[18] mechanistic studies have also shown that the choice of phosphine ligand has a significant impact in determining the course of the reaction.[38,40] Two particular ligand classes that have been used to address this issue

Scheme 1. Intermolecular Hydroacylation

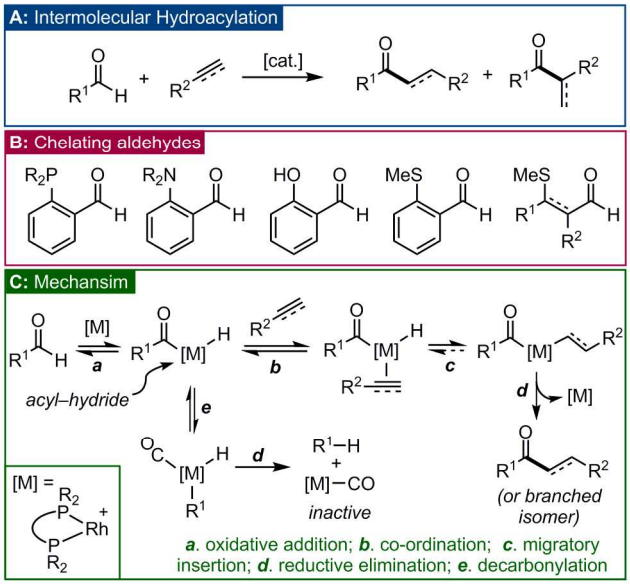

are the small bite angle ligands[41-42] R_2PXPR_2 (R = e.g., ^{t}Bu, *o*-C_6H_4OMe; X = CH_2, NMe_2)[38-39,43] and the hemilabile ligand DPEPhos.[36-37,44-45] Rh-complexes of small bite angle ligands have been shown to be highly active catalysts for the reactions of *β-S*-aldehydes with simple alkenes, alkynes and internal alkenes. Mechanistic studies have indicated that, despite the

Scheme 2. Small bite–angle, DPEPhos and *β*–amido–aldehyde systems

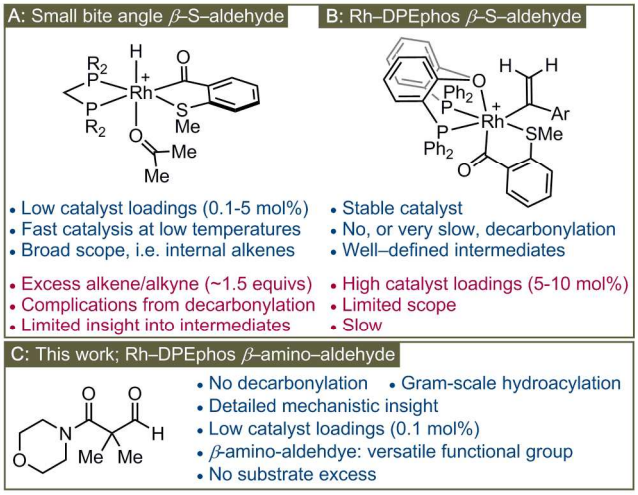

acyl-hydride intermediate (Scheme 2A) undergoing rapid reductive decarbonylation, if the reaction with alkene/alkyne is conducted at appropriately high concentrations, or the resting state is moved away from the acyl-hydride, productive turnover and low catalyst loadings can be achieved, even with challenging substrates, as these ligands have been proposed to promote oxidative addition[17] and reductive elimination.[43,46] Nevertheless, a small excess of alkyne or alkene is required for full conversion (1.3–1.5 equivalents), a requirement that reduces the overall efficiency. Rh-DPEPhos-based catalysts promote the reaction of *β–S*-aldehydes with alkynes/activated alkenes due to the attenuation of decarbonylation, by the stabilization of a 6–coordinate acyl-hydride intermediate by a hemilabile[45] Rh···O interaction. While this removes the *cis*–coordination site necessary for decarbonylation,[36,47] it also results in slow turnover, due to the requirement of a 5–coordinate intermediate for both olefin binding and reductive elimination.[48-49] This limits the substrate scope and results in the requirement of high catalyst loadings for desirable reaction times. Nevertheless, important mechanistic insight arises from these systems, such as the isolation of an intermediate that precedes reductive elimination (Scheme 2B).[40]

While both systems offer benefits neither provide a universal solution, and to develop hydroacylation reactions that could be applied beyond small scale organic synthesis – in areas such as polymer, biological and process chemistries – systems that combine catalyst stability *and* activity are highly desirable. We considered an approach in which the role of the chelating aldehyde in alkyne hydroacylation was explicitly considered. Ideally the aldehyde should: *(i)* offer chelating assistance to aid C–H activation, *(ii)* not be too strongly bound, encouraging alkyne coordination and subsequent reductive elimination, *(iii)* have an α–quaternary centre that would disfavor decarbonylation, and therefore reductive decarbonylation, due to weaker resulting M–CR_3 bonds,[50] *(iv)* deliver a product that does not inhibit turnover by binding strongly.

We settled on *β*-amido-aldehydes as a good starting point, (Figure 2C) and such 1,3-dicarbonyl motifs, and related *β*-ester and *β*-keto-aldehydes, indeed proved to be excellent hydroacylation substrates. Their significant synthetic utility in the construction of hydroacylation adducts, that are themselves powerful synthetic building blocks, has recently been reported by us, and modification of the catalyst identity also allows for control of linear or branched products.[51] We also briefly reported the isolation and solid-state structure of an intermediate in the *β*-amido-aldehydes/alkyne hydroacylation using a moderately active {Rh(Xantphos)}$^+$–based catalyst, [Rh(*mer*–κ^3–$_{P,O,P}$–Xantphos)(H)(COC{$(CH_2)_4$}CO-{NC_4H_8O})][BAr^F_4], (Ar^F = 3,5-$(CF_3)_2C_6H_3$). We also noted a coproduct of a tri–substituted arene that results from a competitive alkyne trimerization in this particular system (Scheme 3).

Scheme 3. Xantphos *β*-amido-acyl-hydride intermediate, hydroacylation and alkyne cyclotrimerization products. [BAr^F_4]$^-$ anions are not shown.

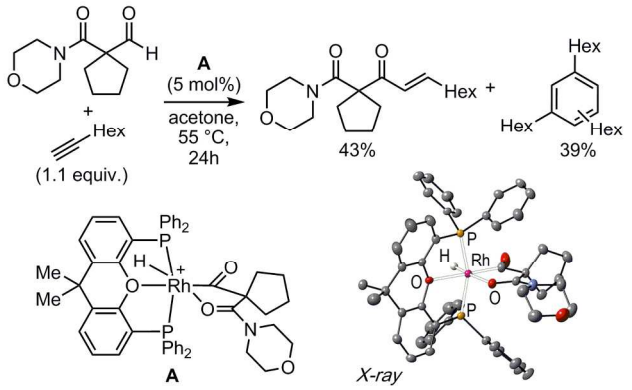

In this contribution we explore, in detail, the mechanism of hydroacylation of *β*-amido–aldehydes with 1–octyne using {Rh(DPEPhos)}$^+$–based catalysts. Through this, we reveal a rich mechanistic landscape of competing hydroacylation and cyclotrimerization reactions; the understanding of which allows for the optimization of productive hydroacylation to essentially quantitative levels, using no excess of either reagent, at very low catalyst loadings, and on gram-scale of product.

2. Results and discussion

2.1 Initial catalysis screening Our pre-catalyst of choice for mechanistic studies is the Rh(I)-complex [Rh(*cis*-κ^2-$_{P,P}$-DPEPhos)(acetone)$_2$][BAr^F_4] **1**,[36-37] which has labile acetone ligands and can be generated *in-situ* by hydrogenation of [Rh(*cis*–κ^2-$_{P,P}$-DPEPhos)(nbd)][BAr^F_4] (nbd = norbornadiene). A catalyst with a weakly bound xylene ligand also works well (see Section 2.10). The reaction between *β*-amido–aldehyde, 2,2-dimethyl-3-morpholino-3-oxopropanal, **2a** (0.75 M) and 1-octyne (**6**) (0.98 M), is catalyzed by **1** (5 mol%, 2 hour, 25 °C) in acetone-d_6 and results in >98% NMR yield of enones **7a**/**7b** (15:1, linear:branched) and a 10% NMR yield of cyclotrimerization products **8a**/**8b** (2:1, 1,2,4-trihexyl benzene: 1,3,5-trihexyl benzene) (Scheme 4). This result demonstrates that pre-catalyst **1** is an effective catalyst and that the conditions deployed are appropriate for more detailed mechanistic study.

Scheme 4. Hydroacylation between aldehyde, 2a, and 1-octyne (6).

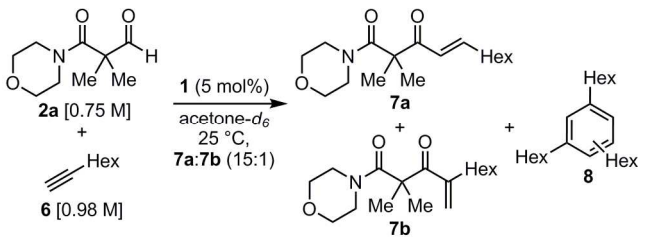

Scheme 5. Synthesis of acyl-hydrides 3a and 3b and reductive decarbonylation. $[BAr^F_4]^-$ anions are not shown.

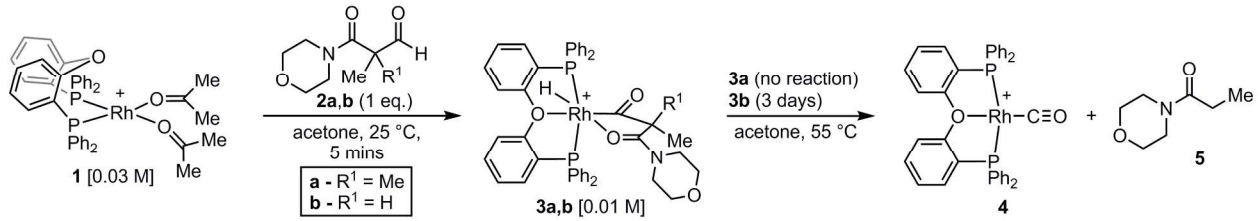

2.2 Speciation and stability studies. The synthesis and stability of intermediate acyl–hydride complexes. Reaction of complex **1** with one equivalent of aldehyde **2a** in acetone–d_6 resulted in the formation, on time of mixing, of the acyl-hydride complex [Rh(*mer*-κ^3-$_{P,O,P}$-DPEPhos)(H)(COC{$(CH_3)_2$}CO-{NC_4H_8O})][BAr^F_4], **3a**, in quantitative yield by NMR spectroscopy. An immediate colour change from red to light yellow occurred signalling the formation of a Rh(III) complex, which was characterized by NMR spectroscopy and ESI–MS (ESI-MS = ElectroSpray Ionization Mass Spectrometry) (Scheme 5).

In the $^{31}P\{^1H\}$ NMR spectrum of complex **3a** a single environment at δ 25.2 [J(RhP) = 127 Hz] is observed, indicating identical phosphorus environments bound to a Rh(III) centre.[52] In the hydride region of the ^1H NMR spectrum, a doublet of triplets is observed at δ –14.6 [J(RhH) = 27.5; J(PH) = 9.5 Hz]. A single methyl environment (relative integral 6 H) is observed for the quaternary centre on the aldehyde. In the $^{13}C\{^1H\}$ NMR spectrum, the acyl-carbon is observed as a doublet of triplets at δ 224.0 [J(RhC) = 37.0; J(PC) = 6.0 Hz]. These data are consistent with an acyl-hydride located *cis* to both phosphines and a *mer*-κ^3 arrangement of the DPEPhos ligand. These spectral features are similar to that of {Rh(Xantphos)}$^+$–complex **A** (Scheme 3) which was shown by single–crystal X-ray crystallography to adopt a *mer*-Xantphos arrangement, with the hydride *trans* to a coordinated amide oxygen and *cis* to the acyl-group. This assignment is also consistent with the structure of the previously reported complex [Rh(*mer*-κ^3-$_{P,O,P}$-DPEPhos)(H)(COCH$_2$CH$_2$SMe)][*closo*-$CB_{11}H_6Cl_6$].[36-37]

Using an aldehyde with a tertiary, rather than a quaternary, center, 2-methyl-3-morpholino-3-oxopropanal **2b**, resulted in the formation of the analogous complex [Rh(*mer*-κ^3-$_{P,O,P}$-DPEPhos)(H)(COC{(CH_3)(H)}CO{NC_4H_8O})][BAr^F_4] **3b**. The resulting NMR data shows the formation of an acyl-hydride, but as there is no longer a mirror plane in the Rh-cation, the $^{31}P\{^1H\}$ NMR spectrum now shows as a tightly–coupled ABX doublet of doublets with a large *trans* ^{31}P–^{31}P coupling:[52] δ 31.3 [J(PP) = 319; J(RhP) = 129 Hz] and δ 22.9 [J(PP) = 319; J(RhP) = 129 Hz]. In the hydride region of the ^1H NMR spectrum, an apparent doublet of triplets at δ –14.9 [J(RhH) = 29.0; J(PH) = 9.0 Hz] is observed. Similarly an apparent doublet of triplets is observed in the $^{13}C\{^1H\}$ NMR at δ 220.3 [J(RhC) = 37.0; J(PC) = 5.5 Hz], which is assigned as the acyl-carbon.

Both complexes **3a** and **3b** are stable for at least 24 hours in acetone-d_6 (0.2 M) as measured by $^{31}P\{^1H\}$ NMR spectroscopy. However, when heated to 55 °C complex **3b** gradually evolved to give the product of reductive decarbonylation [Rh(*mer*-κ^3-$_{P,O,P}$-DPEPhos)(CO)][BAr^F_4], **4**, alongside free 1-morpholinopropan-1-one, **5**. The $^{31}P\{^1H\}$ NMR spectrum of **4** shows a doublet at δ 35 [J(RhP) = 124 Hz], while the ^1H NMR spectrum demonstrates an absence of signals in the hydride region. Complex **4** was also characterized by ESI-MS (m/z = 669.07) and IR spectroscopy ν(CO) = 2017 cm^{-1} (thin film, CD_2Cl_2). The closely related complex [Rh(*mer*-κ^3-$_{P,O,P}$-XantPhos)(CO)][BF_4] has been previously reported, characterized by X-ray crystallography, and shows very similar spectroscopic data to **4** [$^{31}P\{^1H\}$ δ 37, J(RhP) = 122 Hz; ν(CO) = 2014 cm^{-1}].[53-54] [Rh(*cis*-κ^2-$_{P,P}$-DPEPhos)(CO)(EtSMe)][*closo*-$CB_{11}H_6Cl_6$] also results from reductive decarbonylation of the corresponding acylthioether, but in this case the thioether product binds strongly with the metal center unlike amide **5**.[36-37] The increased rate of reductive decarbonylation for aldehyde **2b** compared to aldehyde **2a** demonstrates the postive effect of an α-quaternary center on the stability of intermediate acyl-hydrides, i.e. **3a**.

2.3 Monitoring Catalysis: Kinetics, resting states, competitive late–stage alkyne cyclization and initial rates. An aldehyde that does not undergo reductive decarbonylation provides a rare opportunity to study the mechanism of hydroacylation in the absence of this potentially deleterious process.[13,33-34] Reaction between aldehyde **2a** (0.75 M) and 1-octyne (**6**, 1.3 equivalents, 0.98 M) with **1** (5 mol%, 0.0375M) in acetone-d_6 at 25 °C was monitored by ^1H NMR spectroscopy using the [BAr^F_4]$^-$ anion as an internal reference (Figure 1). 1-octyne (**6**)

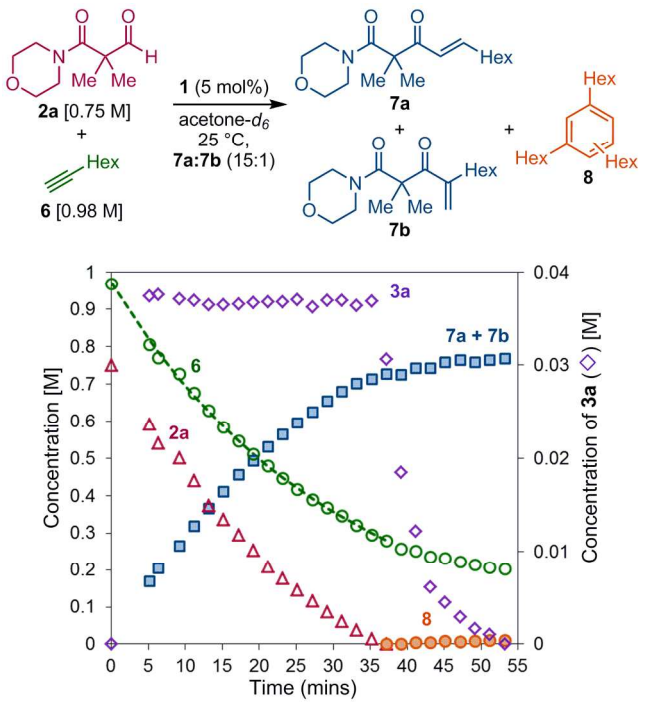

Figure 1. Reaction profile (first 55 minutes) as measured by ^{1}H NMR spectroscopy. Left axis: △ = aldehyde **2a**, ○ = 1- octyne (**6**), ■ = enones **7a** and **7b**, ● = trihexyl benzenes **8**. Dotted green line = first order model for the consumption of 1-octyne (**6**); Right axis: ◇ = acyl-hydride, **3a**.

is consumed by a first order process over three half–lives [k_{obs} = 5.57 (± 0.04) × 10^{-4} s^{-1}], and after 1h a >98% ^{1}H NMR yield of enones **7a**/**7b** (15:1, linear:branched) and a 4% NMR yield of arene cyclotrimerization products **8a**/**8b** (2:1, 1,2,4-trihexyl benzene: 1,3,5-trihexyl benzene) was measured, based upon respective starting materials. During the first 37 minutes of catalysis, the acyl-hydride **3a** was the only organometallic species observed, as determined by ^{31}P{^{1}H} NMR spectroscopy and the distinctive hydride signal at δ –14.6 in the ^{1}H NMR spectrum. The concentration of aldehyde **3a** remains steady over this time (~0.037 M), indicating that reductive decarbonylation does not occur during productive hydroacylation, and that this is the resting state during this period. At ~94% production of the enones **7a**/**7b**, no free aldehyde is observed and the concentration of acyl-hydride **3a** begins to reduce toward zero. This is a pseudo-first order process [k_{obs} = 3.8 (± 0.1) × 10^{-3} s^{-1}] and occurs at the same absolute rate as continued hydroacylation.[55]

Concomitant with the disappearance of acyl-hydride **3a** and complete consumption of free aldehyde **2a**, is continued 1-octyne (**6**) consumption by cyclotrimerization to afford trihexylbenzene products **8** (Figure 1, filled orange circles). This is a relatively slow process so that after 2 hours only a 10% ^{1}H NMR yield is observed, alongside remaining 1-octyne (**6**). Hydroacylation thus initially outcompetes cyclotrimerization, the latter only becoming productive when all free aldehyde is consumed. When this occurs, the resting state changes from acyl-hydride **3a** to one that is characterized by multiple signals between ~δ 24–23 in the ^{31}P{^{1}H} NMR spectrum, and no hydride signal present in the ^{1}H NMR spectrum. This new resting state is explored in more detail later (Section 2.6). The effect of aldehyde and alkyne concentration on the catalytic selectivity was probed by a reaction with an excess of aldehyde **2a** (0.9 M) compared to 1-octyne (**6**, 0.75M). No trihexyl benzenes products **8a**/**8b** were detected and the resting state remained as the acyl-hydride **3a** until complete consumption of 1-octyne (**6**).

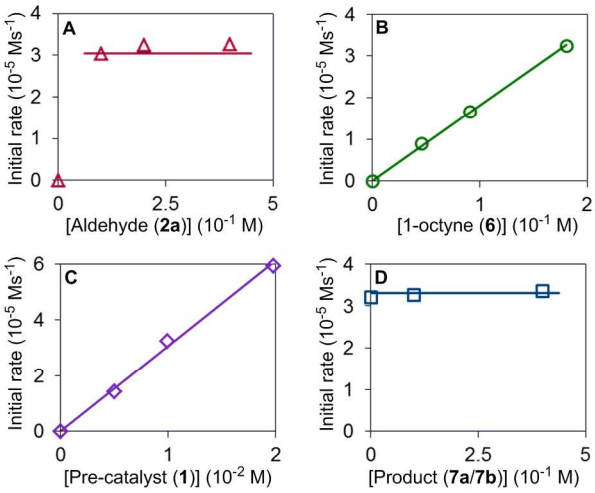

Figure 2. Initial Rate plots for hydroacylation. **A**: Aldehdye (**2a**), ([1–octyne (**6**)] = 0.18 M, [**1**] = 0.01 M); **B**: 1–octyne (**6**), ([aldehyde (**2a**)] = 0.20 M, [**1**] = 0.01 M); **C**: Catalyst (**1**), ([1–octyne (**6**)] = 0.18 M, [aldehyde (**2a**)] = 0.20 M); **D**: Product **7a**/**7b** varied: ([1–octyne (**6**)] = 0.18 M, [aldehyde (**2a**)] = 0.20 M, [**1**] = 0.01 M).

The kinetics of the early-stage hydroacylation catalysis were probed by the initial rates method, monitoring the rate of enones **7a**/**7b** formation using ^{1}H NMR spectroscopy. Figure 2 shows the resulting rate/concentration plots, which demonstrate that catalysis is zero order in aldehyde **2a**, first order in 1-octyne (**6**), and first order in pre-catalyst **1**; the latter observation discounting a dimer–monomer catalyst equilibrium.[56-58] There was no product inhibition even with 40 equivalents of enones **7a**/**7b** relative to **1**. This is in contrast to Rh-small-bite angle catalysts, such as [Rh{^{t}Bu$_2$PCH$_2$P(*o*-C$_6$H$_4$OMe)$_2$}(C$_6$H$_5$F)][BAr$^{F}_4$], which show product inhibition and a product bound-resting state.[39] Together, these observations show that oxidative addition of the aldehyde is fast and strongly favours the Rh(III) acyl-hydride resting state **3a**. From **3a**, alkyne coordination is followed by hydride insertion and reductive elimination, a sequence in which the rate determining step is contained. Product binding is not competitive.

Scheme 6. A. Reaction of 3a with aldehyde (2c); B. Reaction of complex 3a with acetonitrile and aldehyde (2a). [a][BAr$^{F}_4$]$^{-}$ anions are not shown.

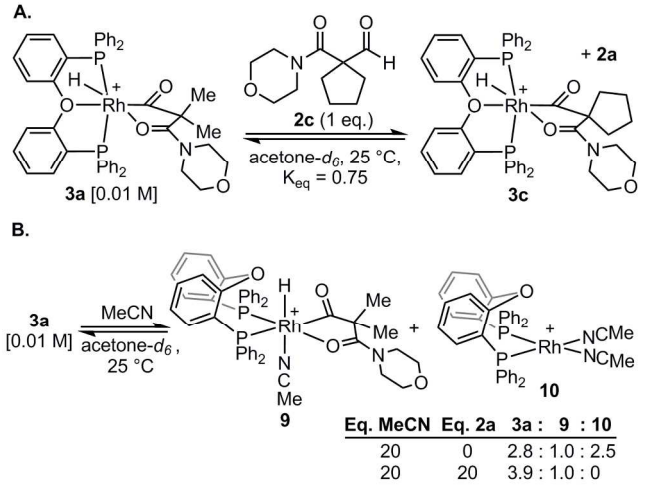

Although following zero-order kinetics in catalysis, the reversibility of aldehyde oxidative addition was probed under stoichiometric conditions by the addition of 1 equivalent of cyclopentyl *β*-amido aldehyde, **2c**, to acyl-hydride **3a**; which resulted in an equilibrium mixture of **3a** and the new acyl-hydride [Rh(*mer*-κ^3-$_{P,O,P}$-DPEPhos)(H)(COC{C_4H_8}CO{NC_4H_8O})] **3c** (K_{eq} = 0.75) on time of mixing (Scheme 6A). Complex **3c** was characterized by ^{1}H NMR spectroscopy which shows a new hydride signal similar to acyl-hydride **3a**, and a ^{31}P{^{1}H} NMR spectrum in which a doublet δ 26.6 [*J*(RhP) = 129 Hz] is observed. This result indicates that oxidative addition of aldehyde is fast and reversible on the reaction timescale. Consistent with this reversibility, addition of 20 equivalents of MeCN to acyl-hydride **3a** resulted in a golden–yellow solution of an equilibrium mixture of **3a** and two new complexes in a 2.8:1.0:2.5 ratio respectively, as measured by ^{31}P{^{1}H} NMR spectroscopy (Scheme 6B and Supporting Materials). One of these new complexes is characterized as Rh(III) [Rh(*cis*-κ^2-$_{P,P}$-DPEPhos)(H)(MeCN)(COC{$(CH_3)_2$}CO{NC_4H_8O})][BAr^F_4], **9**, in which the hemilabile DPEPhos ligand has moved to *cis*–κ^2–P,P coordination mode and the hydride is located *trans* to MeCN. A similar structure has been crystallographically characterized for [Rh(*cis*-κ^2-$_{P,P}$-DPEPhos)(H)(COCH$_2$CH$_2$SMe)(MeCN)][*closo*-$CB_{11}H_6Cl_6$].[37] The third component of the mixture is the Rh(I) complex [Rh(*cis*-κ^2-$_{P,P}$-DPEPhos)(MeCN)$_2$][BAr^F_4], **10**. Free aldehyde, **2a**, is also observed, consistent with the formation of **10**. Addition of aldehyde **2a** (20 equivalents) to this mixture gave a 3.9:1:0 mixture of **3a**:**9**:**10**, demonstrating a system at equilibrium.

Scheme 7. Product bound complex and reactivity with aldehyde. [BAr^F_4]$^-$ anions are not shown.

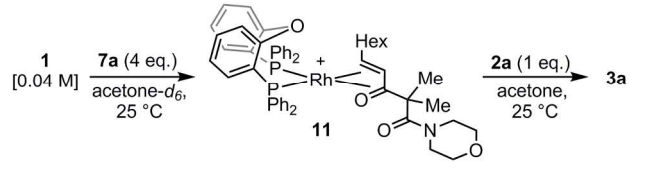

Addition of 4 equivalents of enone **7a** to complex **1** and precipitation from pentane allowed characterization of product-bound Rh(I) complex [Rh(*cis*-κ^2-$_{P,P}$-DPEPhos)(**7a**)][BAr^F_4], **11**, as a dark–red oil, using ^{1}H and ^{31}P{^{1}H} NMR spectroscopy and ESI-MS (Scheme 7). At 298K broad peaks were observed in the ^{31}P{^{1}H} NMR spectrum, which at 190 K resolve into a sharper doublet of doublets at δ 33.0 [J(RhP) = 160; J(PP) = 50 Hz] and δ 25.0 [J(RhP) = 190; J(PP) = 50 Hz]. We suggest this fluxional process is due to a ring-flip of the DPEPhos.[59-60] The ^{1}H NMR spectrum confirmed enone coordination (Supporting Materials). Addition of 1 equivalent of aldehyde **2a** in acetone–d_6 to **11** resulted in an immediate color change to light yellow, and the formation of the acyl-hydride complex **3a** by ^{31}P{^{1}H} NMR spectroscopy. This demonstrates that oxidative addition of aldehyde to the product-bound complex is fast and essentially quantitative, consistent with no product inhibition and the observed acyl-hydride resting state in catalysis.

2.4 Labelling studies and KIE. Kinetic isotope effect (KIE) studies by initial rates on parallel samples, using deuterated aldehyde **2a-*d*$_1$** demonstrated a significant KIE of 1.5 (± 0.1) (Scheme 8A). A KIE close to unity has been reported for an alkyne hydroacylation where reductive bond formation is turnover-limiting.[40] KIEs of between 1.4 and 1.7 have been reported for hydroacylation systems where the turnover-limiting step is proposed to be either hydride insertion, or is reductive bond formation preceded by reversible hydride insertion into an alkene (an equilibrium isotope effect[61-62]).[38-39,43] In reactions where oxidative cleavage of the aldehyde C–H bond

Scheme 8. Labelling Studies and KIE, A. aldehyde-*d*$_1$ (2a-*d*$_1$); B. 1-octyne-*d*$_1$ (6-*d*$_1$).

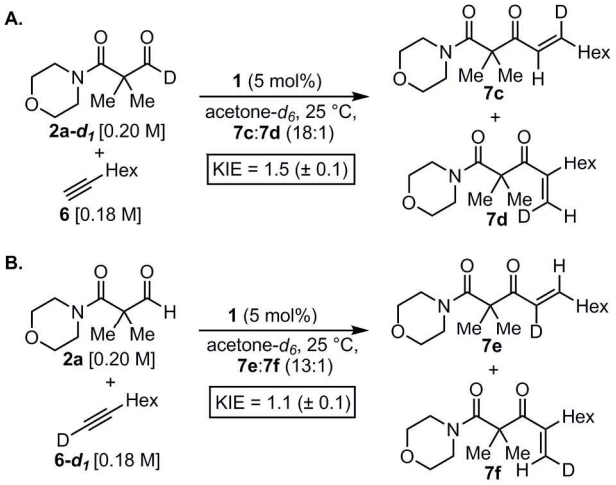

is proposed to be the turnover-limiting step, larger KIE's of 2.4 to 2.9 have been measured.[17-18,58,63] The measured KIE [1.5 (± 0.1)] is also consistent with those reported for hydride insertions into alkenes/alkynes at group 9 metals.[64-65] A KIE of 1.1 (± 0.1) was measured when deuterated 1-octyne **6-*d*$_1$** was used (Scheme 8B) and suggests that C–H activation of the alkyne is not the irreversible rate determining step. Such C–H activation processes have been implicated in the related Ru-catalysed hydroamidation of alkynes, which occur via a vinyldiene intermediate and show KIEs of 1.5–2.3.[66] Based on these observations, hydride insertion is proposed to be turnover-limiting, rather than reductive bond formation, which would be expected to have a KIE close to 1 in the absence of equilibrium isotope effects. We consider such an equilibrium unlikely, as reversible hydride insertion involving alkynes is rare.[64]

These labelling studies also show that deuterium is incorporated into the enone products (**7c-7f**) with a stereochemistry consistent with *syn*–migratory insertion of the hydride into the alkyne. The regiochemistry of the branched products was

found to be selective for one or the other isomer, depending on the use of **2a-*d*$_1$** or **6-*d*$_1$**, and were assigned from selective nOe experiments (Supporting Materials). This selective deuterium incorporation suggests that competitive scrambling of the gem positions, through a metallocyclopropene intermediate, is not occurring; unlike the hydroacylation reactions of 2-(methylthio)benzaldehyde with alkynes catalyzed by $\{Rh(DPEPhos)\}^{+}$ [40] or $\{Rh(^{i}Pr_2P(NMe)P^{i}Pr_2)\}^{+}$ [38] based catalysts.

2.5 Proposed mechanism of hydroacylation and the role of catalyst loading. A mechanism consistent with all the collected data is shown in Scheme 9. Initial reaction of aldehyde **2a** with the bis-acetone pre-catalyst **1** forms the acyl-hydride complex **3a**. Reaction with alkyne (step ***b***), and a change in coordination geometry for the DPEPhos ligand from κ^3 to κ^2, gives intermediate **I** which undergoes turnover-limiting migratory insertion (step ***c***) to form an alkenyl intermediate (**II**). We propose this step is also selectivity determining with regard to

Scheme 9. Proposed hydroacylation mechanism. $[BAr^F_4]^-$ anions are not shown. Only linear pathway shown. TLS = Turnover Limiting Step.

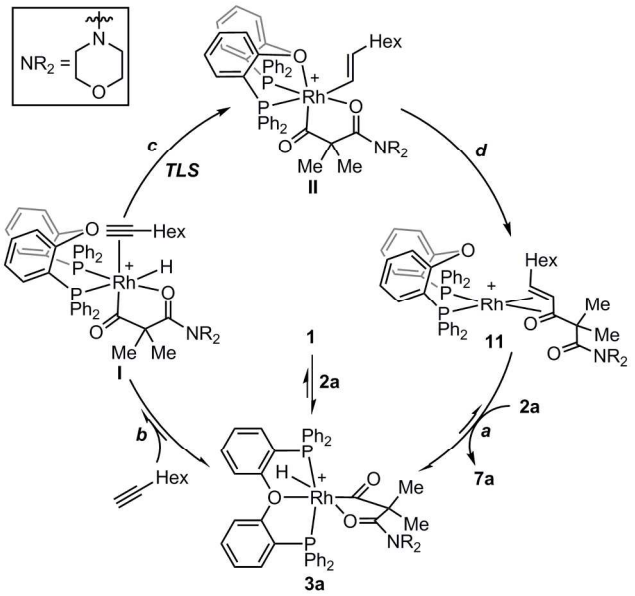

linear/branched isomers. Subsequent reductive bond formation forms enone-bound complex **11** (step ***d***), which is rapidly displaced by additional aldehyde to return **3a** (step ***a***): the observed resting state throughout the reaction until all the aldehyde has been consumed. This strong binding of aldehyde means that at the late stages of hydroacylation all the aldehyde will be bound to the metal centre. When this happens is determined by the relative concentration of catalyst, i.e. at 5 mol% this will occur after 95% of the aldehyde has been consumed. We return to this observation later in the discussion of overall selectivity between hydroacylation and cyclotrimerization.

2.6 Competitive Cyclotrimerization of 1–Octyne. Resting states, initial rate studies and the formation of a coordinated pyran-complex. Cyclotrimerization of 1-octyne (**6**) to form trihexyl benzenes **8a**/**8b** becomes competitive at the later stages of hydroacylation catalysis, when no free aldehyde remains. To study this process in more detail, 1-octyne (**6**) [0.20 M], was reacted with catalyst **1** (5 mol%, 0.01 M) in acetone at 25 °C. This slowly (12 hrs) gave a 66% ^{1}H NMR yield of tri-*n*-hexylbenzene products **8a** and **8b** in a 2:1 ratio (Scheme 10). Complex **1** is immediately consumed at the start of catalysis, and after 5 minutes the organometallic complexes observed by $^{31}P\{^1H\}$ NMR spectroscopy are very similar to those seen in hydroacylation after aldehyde **3a** is consumed (Section 2.2). These are assigned to isomers of the Rh(III)-metallacyclopentadiene [67-68] complex [Rh(*mer*-κ^3-$_{P,O,P}$-DPEPhos)(L)($(CH)_2(C_6H_{13})$)$_2$][BAr^F_4] **12a** (L = 1-octyne). Over time (12 hrs) these resonances decreased in intensity with concomitant increase in the concentration of a new species, characterized as the Rh(I)-pyran complex [Rh(*cis*–κ^2-$_{P,P}$-DPEPhos)(η^2 η^2-2,2-methyl-4,6-*n*-hexyl-α-pyran)][BAr^F_4], **13**.

Scheme 10. Cyclotrimerization of 1-octyne (6) with bis-acetone complex (1) and observed resting states. $[BAr^F_4]^-$ anions are not shown.

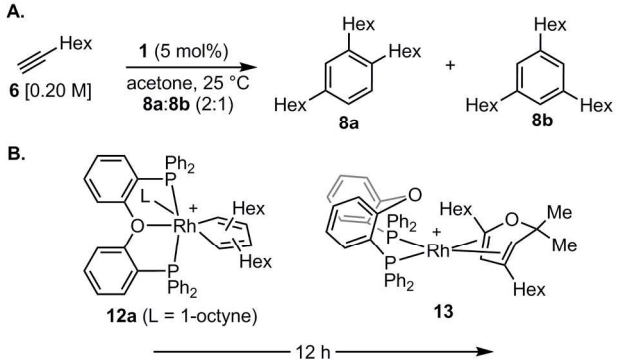

Cyclometallated complexes **12** were characterized *in-situ* at the beginning of catalysis (5 mins). In the $^{31}P\{^1H\}$ NMR spectrum a set of three overlapping broad doublets are observed: δ 23.9 [*J*(RhP) = 125 Hz], δ 23.1 [*J*(RhP) = 130 Hz] and δ 22.9 [*J*(RhP) = 135 Hz]. In the ^{1}H NMR spectrum, multiple signals are observed between δ 5.61 and δ 5.15 assigned to alkenyl groups, while ESI–MS shows a cation containing two 1-octyne (**6**) fragments (*m*/z = 861.29) as the dominant cationic species. These data are consistent with multiple isomers of a Rh(III)-metallacyclopentadiene complex which each have equivalent phosphine environments, but differ in the substitution pattern of the dienyl–fragment. ^{1}H/^{1}H COSY NMR experiments suggest 2,4–, 3,4– and 3,5–hexyl isomers are present. An additional weakly bound ligand at the Rh(III)–centre is suggested, which is likely 1–octyne (**6**) at early stages of catalysis based on the kinetics observed (vide infra), i.e. **12a**. Addition of MeCN (2 equivalents) at this early stage of catalysis results in the three sets of broad signals in $^{31}P\{^1H\}$ NMR spectrum sharpening but not otherwise changing significantly. This suggests that MeCN simply replaces another weakly bound ligand (i.e. 1-octyne) to give [Rh(*mer*-κ^3-$_{P,O,P}$-DPEPhos)(NCMe)($(CH)_2(C(C_6H_{13}))_2$][BAr^F_4], **12c**.

The α-pyran complex **13** that is observed after 12 hours was isolated as a non-crystallisable oil using the $[Al(OC(CF_3)_3)_4]$ anion,[69] and characterized by ^{1}H, ^{13}C, ^{31}P NMR spectroscopy and ESI–MS (*m*/*z* = 919.32). These data suggest a single Rh(I) species with inequivalent phosphines, i.e. δ(^{31}P) 20.8 [*J*(RhP) = 209; *J*(PP) = 31 Hz], δ 17.6 [*J*(RhP) =169; *J*(PP) = 31 Hz]. Detailed NMR spectroscopic analysis (see Supporting Materials) demonstrates that α-pyran is bound to the metal center.[70] α-Pyran coordinated complexes have been previously reported,[71] and the catalytic hetero–cyclotrimerization of diynes with ketones,[72-74] or aryl ethynyl ethers with ketones,[75] to give α-pyrans is known.

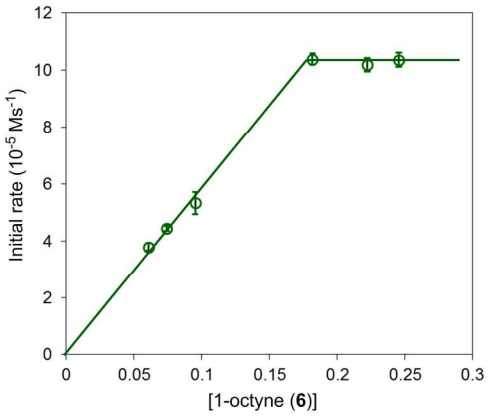

Figure 3. Initial Rates plot for the cyclotrimerization of 1-octyne (**6**) using catalyst 1 (0.01 M).

The kinetics of early stage cyclotrimerization were interrogated by initial rates (Figure 3), in a temporal regime where no pyran-bound complex **13** is observed. Variation of the concentration of 1-octyne (**6**) shows a change in order: at lower concentrations [<0.15 M] first order behaviour is observed, which switches to zero order at higher concentrations [>0.15 M]. When combined with the observation of a metallacyclopentadiene, e.g. **12a**, as the resting state under the early stages of reaction, this allows a mechanism to be proposed (Scheme 11). At higher concentrations of alkyne, initial oxidative coupling of two equivalents of 1-octyne (**6**) with pre-catalyst **1** is followed by quasi-irreversible binding (i.e. saturation kinetics are observed) of a further equivalent of 1-octyne (**6**) to give metallacyclopentadiene **12a.** A subsequent turnover–limiting arene forming process gives the arene-bound complexes of **8a**/**8b**, complex **14**. Rapid displacement of the arene from the metal center by 1-octyne (**6**) then restores the metallacyclopentadiene **12a**. Substituted arenes are labile ligands when partnered with the $\{Rh(DPEPhos)\}^+$ fragment,[76-77] presumably due to the combined electronic and steric effects[78] of the wide-bite angle DPEPhos.[79] At lower concentration of 1-ocytne (**6**) binding of the acetone solvent becomes competitive to form metallacyclopentadiene **12b** (L = acetone) and first order behaviour is observed. Metallacyclopentadiene complexes such as **12** are well established as intermediates in alkyne cyclotrimerzation reactions.[68,80-83]

During this catalysis a competitive [4+2] hetero–cyclotrimerization reaction between 1-octyne (**6**) and acetone solvent occurs to afford the α–pyran complex **13**, exclusively as the 4,6–hexyl–isomer. Selectivity at this step suggests a kinetic preference for the 2,4– and 3,5– isomers of metallacyclopentadiene **12b** reacting with acetone. The so-formed α–pyran ligand binds relatively strongly and therefore becomes the resting state of, and slows, cyclotrimerization catalysis.

Scheme 11. Proposed mechanism of cyclotrimerization of 1-octyne (6). $[BAr^F_4]^-$ anions are not shown. L = solvent (acetone)

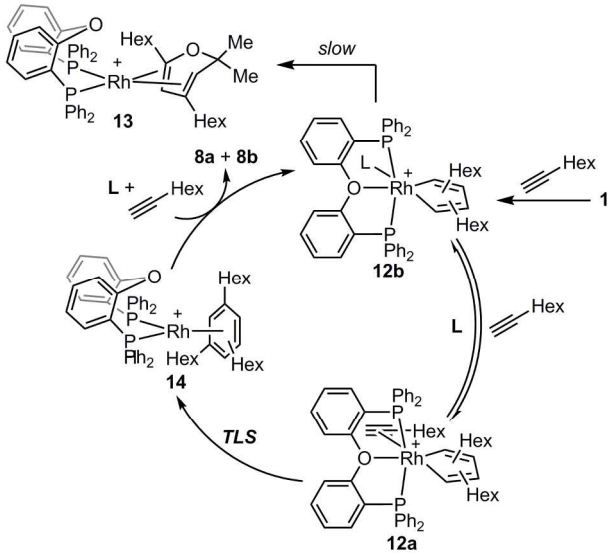

2.7 Moving between catalytic cycles. The efficacy of the isolated α-pyran complex **13** in hydroacylation was investigated using similar conditions as for catalyst **1** ([aldehyde **3a**] = 0.75 M, [1-octyne (**6**)] = 1.5 M, [catalyst **13**] = 0.038 M) and monitored by ^{1}H NMR spectroscopy. The reaction was considerably slower (despite a higher concentration of alkyne), taking 3 hours to achieve full consumption of aldehyde, at which point cyclotrimerization began. Monitoring the rhodium-speciation by ^{1}H NMR spectroscopy revealed a slow conversion of the pyran-bound complex **13** to the acyl hydride **3a**, with no other rhodium complexes being observed (See Supporting Materials). This suggests that the α–pyran ligand is relatively strongly bound to the Rh(I) center.

The movement from the cyclotrimerization cycle to hydroacylation was confirmed by the addition of aldehyde **2a** to the pre-formed metallacyclopentadiene **12a** (in the presence of excess alkyne). This resulted in the slow formation of acyl-hydride **3a**, presumably via slow cyclotrimerization to form tri-*n*-hexyl-benzene complex **14**, which then rapidly reacts with aldehyde. Enone-bound complex **11** can also enter into the cyclotrimerization manifold, as shown by reaction with 1-octyne (**6**) (20 equivalents, 0.20 M, acetone–d_6) that forms a mixture of **11** and **12a** which after 25 minutes is fully converted to a mixture of metallacyclopentadiene **12** and α-pyran complex **13** with concomitant formation of tri-*n*-hexyl-benzene.

2.8 Summary of the overall mechanism. Scheme 12 presents an overview of the various processes occurring when pre-catalyst **1** is combined with aldehyde **2a** and alkyne **6**. The resting state of hydroacylation (cycle A) is acyl-hydride **3a**, due to strong aldehyde binding (zero order kinetics), and the rate determining step is proposed to be hydride insertion. When the concentration of free aldehyde approaches zero, cyclotrimerization (cycle B) becomes competitive. At this point, when the remaining acyl hydride **3a** turns over in hydroacylation there is no aldehyde left to reform it, and with free alkyne now effectively in excess, the resting state moves to the metallacyclopentadiene, e.g. **12a**, likely via enone–bound complex **11**. Addition of aldehyde **2a** moves the resting state back to acyl-hydride **3a**, albeit slowly as the pathways from metallacyclopentadiene **12** or α–pyran complex **13** are sluggish. Consistent with this, recharging experiments show productive catalysis occurs, but now an induction period was

observed (Supporting Materials) during which the resting state moves from **12**/**13** to **3a**.

Scheme 12. Overall mechanistic landscape. $[BAr^F_4]^-$ anions are not shown.

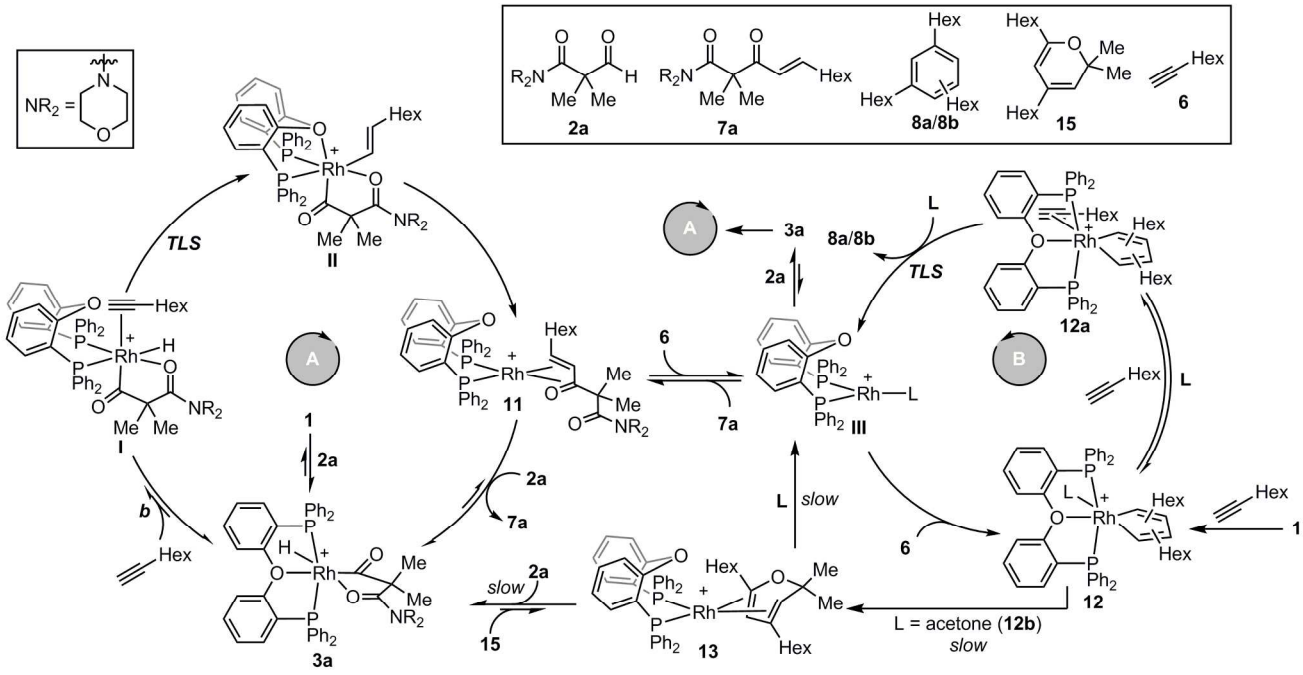

2.9 Role of relative concentrations of aldehyde, alkyne and catalyst in determining selectivity. These observations show that movement between the two catalytic regimes of hydroacylation and cyclotrimerization is rather straightforward and is biased by relative rates of reaction and concentration of substrates. Interested in developing a process selective for hydroacylation (i.e., no cyclotrimerization) the optimization of conditions was studied – armed with the detailed knowledge of the catalytic cycles operating. The late stages of hydroacylation were modelled by addition of one equivalent of 1-octyne (**6**) to acyl hydride **3a**. After 3h a 33% yield of enones **7a**/**7b** and a 54% yield of tri-*n*-hexyl-benzenes **8** were measured by ^{1}H NMR spectroscopy (Figure 4, **A**). In the ^{31}P{^{1}H} NMR spectrum a mixture of bis-acetone complex **1**, acyl hydride **3a** and α-pyran-complex **13** were present in the relative ratio of 1:2:1 respectively. Performing the same reaction with an added equivalent of aldheyde **2a**, a 97% yield of enones **7a**/**7b** was observed, with only traces of cyclotrimerization detected (Figure 4, **B**); the only complex observed by ^{31}P{^{1}H} NMR spectroscopy was acyl-hydride **3a**. The important conclusions that arise from this are: *(i)* cyclotrimerization only becomes competitive when there is no aldehyde present in solution; *(ii)* as aldehyde binds so strongly to form acyl-hydride **3a** (recall zero-order kinetics) the point where this happens will directly correlate to catalyst loading, with low loadings allowing for free aldehyde to be present for longer.

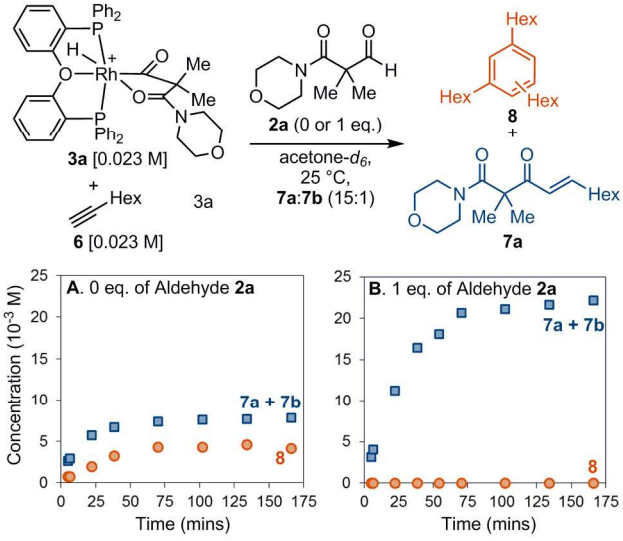

Figure 4. Reaction profile as measured by ^{1}H NMR spectroscopy, **A**. 0 equivalents of aldehyde **2a**; **B**. 1 equivalent of aldehyde: ■ □ = enones **7a** and **7b**, ● = trihexyl-benzenes **8**.

A study of relative concentrations and catalyst loadings was then performed (Table 1). With an excess of 1-octyne (**6**), a selectivity for hydroacylation of 92% was determined (Entry 1). An excess of aldehyde gave a selectivity of 100% for hydroacylation (Entry 2), but a reduction in overall atom economy. At a more favourable 1:1 aldehyde to alkyne ratio and a catalyst loading of 20 mol% a selectivity to 96% was measured, with a hydroacylation yield of 96% (Entry 3). This is because at 80% enone (**7**) formation all remaining aldehyde is bound to the metal center as acyl-hydride **3a**. As this turns over, cyclotrimerization with the remaining free 1-octyne (**6**)

becomes competetive, and selectivity drops. Reducing the catalyst loading should move this tipping point later. At 2.5 mol% loading of **1** a selectivity of 99% is thus measured (Entry 4), while at 0.5 mol% essentially 100% selectivity (Entry 5) is achieved using equimolar amounts of starting materials. This is a remarkable result, as the highest selectivity, and maximum atom-economy of products from reagents, comes from the lowest catalyst loading and no excess of either substrate.

Table 1. Optimization of selectivity between hydroacylation and cyclotrimerization

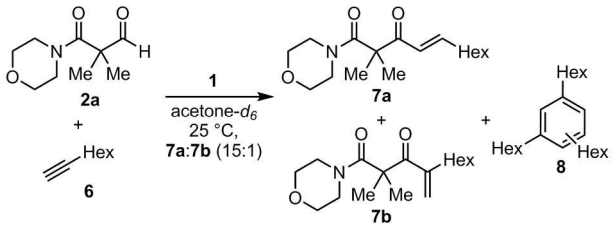

Entry	[**2a**] (M)	[**6**] (M)	**1** (mol%)	**7a**/**7b** (%)[a,b]	**8a**/**8a** (%)[b,c]	**7**:**8** (%)[d]
1	0.75	0.98	5.0	>98	9	92
2	0.9	0.75	5.0	>98	0	100
3	0.75	0.75	20	96	4	96
4	0.75	0.75	2.5	>98	1	99
5	0.75	0.75	0.5	>98	0	100

[a]^{1}H NMR yield based on limiting reagent; [b]using 1,2,4,5-teteachloro-3-nitobenzene as an internal standard; [c]^{1}H NMR yield based on available alkyne, [d]% yield of **7a**/**7b** compared to **8a**/**8b**.

2.10 Developing a highly selective hydroacylation reaction on scale. With such a robust, selective and efficient hydroacylation system in hand the opportunity to scale up to gram-quantities presented an exciting possibility. To do this, the pyrrolidine aldehyde **2c** was used as a coupling partner, as it is a solid at room temperature (unlike liquid **2a**) making handling on scale easier (see Supporting Materials for the synthesis of **2c** on a decagram scale in 63% overall yield). The previously reported catalyst precursor [Rh(*mer*-κ^2-$_{P,P}$-DPEPhos)(*o*-xylene)][BAr$^F{}_4$] **16** was used.[76] This has the advantage over **1** that it does not require hydrogenation before use in catalysis, is bench stable (> 6 months), and the labile arene ligand allows for rapid and quantitative reaction with aldehyde to form acyl-hydrides, e.g **3a** (Supporting Materials). A design of experiments methodology was used for optimization of the catalysis, in which temperature and concentration were varied. Each reaction was run on a 0.5 g scale, using a 1:1 ratio of aldehyde **2c**, 1-octyne (**6**) and 0.5 mol% **16**. Reaction progress was monitored by gas chromatography. Over the concentration/temperature range tested (1.20 to 3.46 M and 10 to 31.5 °C) yields of >98% and selectivity of 100% were measured in all cases, demonstrating the efficacy of the catalyst. For all scenarios a pseudo first–order rate law was obtained for the first two half-lives of the reaction (cf Figure 1), showing that the gross kinetics of the reactions are unchanged despite the change in conditions (Supporting Materials).

Conditions of highest temperature and concentration where thus chosen so to minimise reaction time (30 °C, 3.3 M), and these were then employed for the synthesis of **17a**/**17b** on large scale (5 g). The reaction was measured to be complete by GC after 3 hours. Simple precipitation of the catalyst from the reaction by addition of heptane followed by filtration through a plug of silica (workup conditions not optimized) resulted in a 97% isolated yield of **17a**/**17b** (11:1) with >98% NMR purity. As this Rh–catalyzed hydroacylation is an atom–efficient catalytic process, when coupled with the high concentrations of substrates used (and thus minimal acetone solvent, ~ 4 g) it results in an exceptionally efficient reaction for the large–scale reaction, as described in Scheme 13.

Scheme 13. Large scale reaction

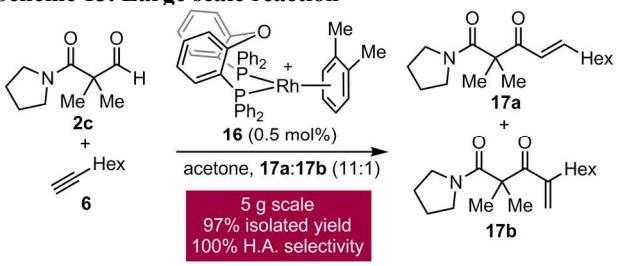

The Process Mass Intensity (PMI)[84] is the ratio of the total input mass in a process (including catalysts and solvents) compared to the mass of isolated product. A desirable PMI is one that approaches 1; a special case which would use no solvent or catalyst and would also be 100% atom-efficient. The hydroacylation process described approaches many of these desirable attributes, including a 1:1 ratio of aldehyde to alkyne, low catalyst loadings, and high yields/selectivity that allow for simple purification that avoids column chromatography. This is in addition to the modest temperature and short reaction times. For these conditions we estimate a PMI = 30. This metric can be compared with an equivalent hydroacylation process reported for similar substrates and catalysts, for which we estimate to have a PMI = 330, an order of magnitude difference,[51] as these procedures use lower substrate concentrations, have lower isolated yields and require column chromatography. Our conditions were also tested at lower catalyst loadings (0.1 mol%) under otherwise identical conditions but on a smaller scale (0.5 g), and afforded a 91% isolated yield of enones **17** after 24 h, further demonstrating the stability of the catalytic system.

3. Conclusions. The drive for perfect selectivity in catalytic processes leads to attendant increases in overall processes efficiencies, and reduced materials and energy costs. As industrial chemical separations account for 10–15% of global energy demand[85] such considerations are becoming increasingly important. In this regard the hydroacylation reaction represents an ideal target for further optimization as it is, in principle, already a 100% atom efficient process. We demonstrate that through correct substrate choice and detailed mechanistic studies, a process that is essentially 100% selective for hydroacylation can be developed that requires no excess of either reagent, operates best at low absolute catalyst loadings, uses minimal solvent, needs virtually no workup and delivers gram scales of product. This encourages the future development of hydroacylation as a cross–coupling technique for the production of fine and commodity chemicals and intermediates.

AUTHOR INFORMATION

Corresponding Author

*andrew.weller@chem.ox.ac.uk

ORCID

Andrew S. Weller: 0000-0003-1646-8081

Michael C. Willis: 0000-0002-0636-6471

Author Contributions

All authors have given approval to the final version of the manuscript.

Notes

The authors declare no competing financial interest.

Supporting Information.

The Supporting Information is available free of charge on the ACS Publications website at DOI:.

Experimental and characterization details, including NMR spectroscopic and kinetic data.

ACKNOWLEDGMENT

This work was supported by the EPSRC (EP/K024205/1, EP/M024210/1), the EPSRC Centre for Doctoral Training in Synthesis for Biology and Medicine (EP/L015838/1, to J.B.-S.). Louisa Britton is thanked for preliminary studies.

REFERENCES

(1) Jun, C. H.; Jo, E. A.; Park, J. W. Intermolecular hydroacylation by transition-metal complexes, *Eur. J. Org. Chem.* **2007**, 1869-1881.

(2) Ghosh, A.; Johnson, K. F.; Vickerman, K. L.; Walker, J. A.; Stanley, L. M. Recent advances in transition metal-catalysed hydroacylation of alkenes and alkynes, *Org. Chem. Front.* **2016**, *3*, 639-644.

(3) Omura, S.; Fukuyama, T.; Horiguchi, J.; Murakami, Y.; Ryu, I. Ruthenium Hydride-Catalyzed Addition of Aldehydes to Dienes Leading to β,γ-Unsaturated Ketones, *J. Am. Chem. Soc.* **2008**, *130*, 14094-14095.

(4) Williams, V. M.; Leung, J. C.; Patman, R. L.; Krische, M. J. Hydroacylation of 2-butyne from the alcohol or aldehyde oxidation level via ruthenium catalyzed C-C bond forming transfer hydrogenation, *Tetrahedron* **2009**, *65*, 5024-5029.

(5) Shibahara, F.; Bower, J. F.; Krische, M. J. Diene Hydroacylation from the Alcohol or Aldehyde Oxidation Level via Ruthenium-Catalyzed C-C Bond-Forming Transfer Hydrogenation: Synthesis of β,γ-Unsaturated Ketones, *J. Am. Chem. Soc.* **2008**, *130*, 14120-14122.

(6) Chen, Q. A.; Cruz, F. A.; Dong, V. M. Alkyne Hydroacylation: Switching Regioselectivity by Tandem Ruthenium Catalysis, *J. Am. Chem. Soc.* **2015**, *137*, 3157-3160.

(7) Kim, J.; Yi, C. S. Intermolecular Markovnikov-Selective Hydroacylation of Olefins Catalyzed by a Cationic Ruthenium-Hydride Complex, *ACS Catal.* **2016**, *6*, 3336-3339.

(8) Tsuda, T.; Kiyoi, T.; Saegusa, T. Nickel(0)-Catalyzed Hydroacylation of Alkynes with Aldehydes to α,β-Enones, *J. Org. Chem.* **1990**, *55*, 2554-2558.

(9) Xiao, L. J.; Fu, X. N.; Zhou, M. J.; Xie, J. H.; Wang, L. X.; Xu, X. F.; Zhou, Q. L. Nickel-Catalyzed Hydroacylation of Styrenes with Simple Aldehydes: Reaction Development and Mechanistic Insights, *J. Am. Chem. Soc.* **2016**, *138*, 2957-2960.

(10) Lenges, C. P.; Brookhart, M. Co(I)-catalyzed inter- and intramolecular hydroacylation of olefins with aromatic aldehydes, *J. Am. Chem. Soc.* **1997**, *119*, 3165-3166.

(11) Chen, Q. A.; Kim, D. K.; Dong, V. M. Regioselective Hydroacylation of 1,3-Dienes by Cobalt Catalysis, *J. Am. Chem. Soc.* **2014**, *136*, 3772-3775.

(12) Marder, T. B.; Roe, D. C.; Milstein, D. Transition-Metal-Catalyzed C-C Bond Formation via C-H Activation - Intermolecular Hydroacylation - the Addition of Aldehydes to Alkenes, *Organometallics* **1988**, *7*, 1451-1453.

(13) Roy, A. H.; Lenges, C. P.; Brookhart, M. Scope and mechanism of the intermolecular addition of aromatic aldehydes to olefins catalyzed by Rh(I) olefin complexes, *J. Am. Chem. Soc.* **2007**, *129*, 2082-2093.

(14) Tanaka, K.; Shibata, Y.; Suda, T.; Hagiwara, Y.; Hirano, M. Direct Intermolecular Hydroacylation of N,N-Dialkylacrylamides with Aldehydes Catalyzed by a Cationic Rhodium(I)/dppb Complex, *Org. Lett.* **2007**, *9*, 1215-1218.

(15) Shibata, Y.; Tanaka, K. Rhodium-Catalyzed Highly Enantioselective Direct Intermolecular Hydroacylation of 1,1-Disubstituted Alkenes with Unfunctionalized Aldehydes, *J. Am. Chem. Soc.* **2009**, *131*, 12552-12553.

(16) Murphy, S. K.; Bruch, A.; Dong, V. M. Substrate-Directed Hydroacylation: Rhodium-Catalyzed Coupling of Vinylphenols and Nonchelating Aldehydes, *Angew. Chem. Int. Ed.* **2014**, *53*, 2455-2459.

(17) Murphy, S. K.; Bruch, A.; Dong, V. M. Mechanistic insights into hydroacylation with non-chelating aldehydes, *Chem. Sci.* **2015**, *6*, 174-180.

(18) Guo, R.; Zhang, G. Z. Expedient Synthesis of 1,5-Diketones by Rhodium-Catalyzed Hydroacylation Enabled by C-C Bond Cleavage, *J. Am. Chem. Soc.* **2017**, *139*, 12891-12894.

(19) Lee, H.; Jun, C. H. Hydroacylation of 1-Alkene with 2-(Diphenylphosphino)benzaldehyde by Rh(I), *Bull. Korean Chem. Soc.* **1995**, *16*, 66-68.

(20) Vora, K. P.; Lochow, C. F.; Miller, R. G. Rhodium Catalyzed Hydroacylation of Ethylene with 4-Pentenals - Reactions of 4-Hexenal-1-*d*, *J. Organomet. Chem.* **1980**, *192*, 257-264.

(21) Castaing, M.; Wason, S. L.; Estepa, B.; Hooper, J. F.; Willis, M. C. 2-Aminobenzaldehydes as Versatile Substrates for Rhodium-Catalyzed Alkyne Hydroacylation: Application to Dihydroquinolone Synthesis, *Angew. Chem. Int. Ed.* **2013**, *52*, 13280-13283.

(22) Zhang, T.; Qi, Z. S.; Zhang, X. Y.; Wu, L. M.; Li, X. W. Rh^{III}-Catalyzed Hydroacylation Reactions between *N*-Sulfonyl 2-Aminobenzaldehydes and Olefins, *Chem. Eur. J.* **2014**, *20*, 3283-3287.

(23) Kokubo, K.; Matsumasa, K.; Miura, M.; Nomura, M. Rhodium-Catalyzed Coupling Reaction of Salicyl Aldehydes with Alkynes via Cleavage of the Aldehyde C-H Bond, *J. Org. Chem.* **1997**, *62*, 4564-4565.

(24) Imai, M.; Tanaka, M.; Tanaka, K.; Yamamoto, Y.; Imai-Ogata, N.; Shimowatari, M.; Nagumo, S.; Kawahara, N.; Suemune, H. Double-Chelation-Assisted Rh-Catalyzed Intermolecular Hydroacylation between Salicylaldehydes and 1,4-penta- or 1,5-hexadienes, *J. Org. Chem.* **2004**, *69*, 1144-1150.

(25) Coulter, M. M.; Kou, K. G. M.; Galligan, B.; Dong, V. M. Regio- and Enantioselective Intermolecular Hydroacylation: Substrate-Directed Addition of Salicylaldehydes to Homoallylic Sulfides, *J. Am. Chem. Soc.* **2010**, *132*, 16330-16333.

(26) Murphy, S. K.; Petrone, D. A.; Coulter, M. M.; Dong, V. M. Catalytic Hydroacylation as an Approach to Homoaldol Products, *Org. Lett.* **2011**, *13*, 6216-6219.

(27) Du, X. W.; Stanley, L. M. Tandem Alkyne Hydroacylation and Oxo-Michael Addition: Diastereoselective Synthesis of 2,3-Disubstituted Chroman-4-ones and Fluorinated Derivatives, *Org. Lett.* **2015**, *17*, 3276-3279.

(28) Willis, M. C.; McNally, S. J.; Beswick, P. J. Chelation-Controlled Intermolecular Hydroacylation: Direct Addition of Alkyl Aldehydes to Functionalized Alkenes, *Angew. Chem. Int. Ed.* **2004**, *43*, 340-343.

(29) Willis, M. C.; Randell-Sly, H. E.; Woodward, R. L.; Currie, G. S. Chelation-Controlled Intermolecular Alkene and Alkyne Hydroacylation: The Utility of β-Thioacetal Aldehydes, *Org. Lett.* **2005**, *7*, 2249-2251.

(30) Osborne, J. D.; Randell-Sly, H. E.; Currie, G. S.; Cowley, A. R.; Willis, M. C. Catalytic Enantioselective Intermolecular Hydroacylation: Rhodium-Catalyzed Combination of β-S-Aldehydes and 1,3-Disubstituted Allenes, *J. Am. Chem. Soc.* **2008**, *130*, 17232-17233.

(31) Parsons, S. R.; Hooper, J. F.; Willis, M. C. *O*-Substituted Alkyl Aldehydes for Rhodium-Catalyzed Intermolecular Alkyne Hydroacylation: The Utility of Methylthiomethyl Ethers, *Org. Lett.* **2011**, *13*, 998-1000.

(32) Hooper, J. F.; Seo, S.; Truscott, F. R.; Neuhaus, J. D.; Willis, M. C. α-Amino Aldehydes as Readily Available Chiral Aldehydes for Rh-Catalyzed Alkyne Hydroacylation, *J. Am. Chem. Soc.* **2016**, *138*, 1630-1634.
(33) Fairlie, D. P.; Bosnich, B. Homogeneous Catalysis - Mechanism of Catalytic Hydroacylation - the Conversion of 4-Pentenals to Cyclopentanones, *Organometallics* **1988**, *7*, 946-954.
(34) Fairlie, D. P.; Bosnich, B. Homogeneous Catalysis - Conversion of 4-Pentenals to Cyclopentanones by Efficient Rhodium-Catalyzed Hydroacylation, *Organometallics* **1988**, *7*, 936-945.
(35) Milstein, D. Isolation and Direct Observation of Intramolecular Hydroacylation of a *cis*-hydridopent-4-enoylrhodium(III) Complex, *J. Chem. Soc. Chem. Comm.* **1982**, 1357-1358.
(36) Moxham, G. L.; Randell-Sly, H. E.; Brayshaw, S. K.; Woodward, R. L.; Weller, A. S.; Willis, M. C. A Second-Generation Catalyst for Intermolecular Hydroacylation of Alkenes and Alkynes Using β-S-substituted aldehydes: The role of a Hemilabile P-O-P ligand, *Angew. Chem. Int. Ed.* **2006**, *45*, 7618-7622.
(37) Moxham, G. L.; Randell-Sly, H.; Brayshaw, S. K.; Weller, A. S.; Willis, M. C. Intermolecular Alkene and Alkyne Hydroacylation with β-S-Substituted Aldehydes: Mechanistic Insight into the Role of a Hemilabile P-O-P Ligand, *Chem. Eur. J.* **2008**, *14*, 8383-8397.
(38) Pernik, I.; Hooper, J. F.; Chaplin, A. B.; Weller, A. S.; Willis, M. C. Exploring Small Bite-Angle Ligands for the Rhodium-Catalyzed Intermolecular Hydroacylation of β-S-Substituted Aldehydes with 1-Octene and 1-Octyne, *ACS Catal.* **2012**, *2*, 2779-2786.
(39) Prades, A.; Fernandez, M.; Pike, S. D.; Willis, M. C.; Weller, A. S. Well-Defined and Robust Rhodium Catalysts for the Hydroacylation of Terminal and Internal Alkenes, *Angew. Chem. Int. Ed.* **2015**, *54*, 8520-8524.
(40) Pawley, R. J.; Huertos, M. A.; Lloyd-Jones, G. C.; Weller, A. S.; Willis, M. C. Intermolecular Alkyne Hydroacylation. Mechanistic Insight from the Isolation of the Vinyl Intermediate That Precedes Reductive Elimination, *Organometallics* **2012**, *31*, 5650-5659.
(41) Schultz, M.; Eisentrager, F.; Regius, C.; Rominger, F.; Hanno-Igels, P.; Jakob, P.; Gruber, I.; Hofmann, P. Crowded Diphosphinomethane Ligands in Catalysis: $[(R_2PCH_2PR'_2\text{-}k^2P)\text{-}NiR']^+$ Cations for Ethylene Polymerization without Activators, *Organometallics* **2012**, *31*, 207-224.
(42) Mansell, S. M. Catalytic applications of small bite-angle diphosphorus ligands with single-atom linkers, *Dalton. Trans.* **2017**, *46*, 15157-15174.
(43) Chaplin, A. B.; Hooper, J. F.; Weller, A. S.; Willis, M. C. Intermolecular Hydroacylation: High Activity Rhodium Catalysts Containing Small-Bite-Angle Diphosphine Ligands, *J. Am. Chem. Soc.* **2012**, *134*, 4885-4897.
(44) Pawley, R. J.; Moxham, G. L.; Dallanegra, R.; Chaplin, A. B.; Brayshaw, S. K.; Weller, A. S.; Willis, M. C. Controlling Selectivity in Intermolecular Alkene or Aldehyde Hydroacylation Reactions Catalyzed by $\{Rh(L_2)\}^+$ Fragments, *Organometallics* **2010**, *29*, 1717-1728.
(45) Adams, G. M.; Weller, A. S. POP-type ligands: Variable coordination and hemilabile behaviour, *Coord. Chem. Rev.* **2018**, *355*, 150-172.
(46) Reid, S. M.; Mague, J. T.; Fink, M. J. Facile Reductive Elimination of Ethane from Strained Dimethylpalladium(II) Complexes, *J. Am. Chem. Soc.* **2001**, *123*, 4081-4082.
(47) Goikhman, R.; Milstein, D. Ligand-Controlled Chemoselectivity in the Classical Oxidative Addition Reactions of MeI and Aldehydes to Rhodium(I) Complexes, *Angew. Chem. Int. Ed.* **2001**, *40*, 1119-1120.
(48) Luedtke, A. T.; Goldberg, K. I. Reductive Elimination of Ethane from Five-Coordinate Platinum(IV) Alkyl Complexes, *Inorg. Chem.* **2007**, *46*, 8496-8498.
(49) Hartwig, J. F. *Organotransition Metal Chemistry: From Bonding to Catalysis*; University Science Books, 2010.
(50) Uddin, J.; Morales, C. M.; Maynard, J. H.; Landis, C. R. Computational Studies of Metal-Ligand Bond Enthalpies across the Transition Metal Series, *Organometallics* **2006**, *25*, 5566-5581.
(51) Coxon, T. J.; Fernandez, M.; Barwick-Silk, J.; McKay, A. I.; Britton, L. E.; Weller, A. S.; Willis, M. C. Exploiting Carbonyl Groups to Control Intermolecular Rhodium-Catalyzed Alkene and Alkyne Hydroacylation, *J. Am. Chem. Soc.* **2017**, *139*, 10142-10149.
(52) Pregosin, P. S. *NMR in Organometallic Chemistry*; Wiley VCH, 2012.
(53) Sandee, A. J.; van der Veen, L. A.; Reek, J. N. H.; Kamer, P. C. J.; Lutz, M.; Spek, A. L.; van Leeuwen, P. W. N. M. A robust, Environmentally Benign Catalyst for Highly Selective Hydroformylation, *Angew. Chem. Int. Ed.* **1999**, *38*, 3231-3235.
(54) Williams, G. L.; Parks, C. M.; Smith, C. R.; Adams, H.; Haynes, A.; Meijer, A. J. H. M.; Sunley, G. J.; Gaemers, S. Mechanistic Study of Rhodium/xantphos-Catalyzed Methanol Carbonylation, *Organometallics* **2011**, *30*, 6166-6179.
(55) After free aldehyde consumption (37-43 mins), the absolute rate of hydroacylation; as measured by product formation, is, within error, the same as that of acyl hydride consumption; $6 (\pm 1) \times 10^{-5}$ Ms^{-1} and $7 (\pm 1) \times 10^{-5}$ Ms^{-1} respectively. This is consistent with the forward hydroacylation process, from acyl-hydride **3a** to give alkyne-bound intermediate (**I**, Scheme 9), being the dominant pathway for acyl-hydride consumption. The respective, calculated, second order rate constants follow the same trend ($k = 1.6 (\pm 0.1) \times 10^{-2}$ $M^{-1}s^{-1}$, $k = 1.5 (\pm 0.4) \times 10^{-2}$ $M^{-1}s^{-1}$).
(56) van Strijdonck, G. P. F.; Boele, M. D. K.; Kamer, P. C. J.; de Vries, J. G.; van Leeuwen, P. W. N. M. Fast Palladium Catalyzed Arylation of Alkenes Using Bulky Monodentate Phosphorus Ligands, *Eur. J. Inorg. Chem.* **1999**, 1073-1076.
(57) Sewell, L. J.; Huertos, M. A.; Dickinson, M. E.; Weller, A. S.; Lloyd-Jones, G. C. Dehydrocoupling of Dimethylamine Borane Catalyzed by $Rh(PCy_3)_2H_2Cl$, *Inorg. Chem.* **2013**, *52*, 4509-4516.
(58) Kou, K. G. M.; Le, D. N.; Dong, V. M. Rh(I)-Catalyzed Intermolecular Hydroacylation: Enantioselective Cross-Coupling of Aldehydes and Ketoamides, *J. Am. Chem. Soc.* **2014**, *136*, 9471-9476.
(59) Goertz, W.; Keim, W.; Vogt, D.; Englert, U.; Boele, M. D. K.; van der Veen, L. A.; Kamer, P. C. J.; van Leeuwen, P. W. N. M. Electronic effects in the nickel-catalysed hydrocyanation of styrene applying chelating phosphorus ligands with large bite angles, *J. Chem. Soc. Dalton Trans.* **1998**, 2981-2988.
(60) Pingen, D.; Lebl, T.; Lutz, M.; Nichol, G. S.; Kamer, P. C. J.; Vogt, D. Catalytic Activity and Fluxional Behavior of Complexes Based on $RuHCl(CO)(PPh_3)_3$ and Xantphos-Type Ligands, *Organometallics* **2014**, *33*, 2798-2805.
(61) Jones, W. D. Isotope Effects in C-H Bond Activation Reactions by Transition Metals, *Acc. Chem. Res.* **2003**, *36*, 140-146.
(62) Simmons, E. M.; Hartwig, J. F. On the Interpretation of Deuterium Kinetic Isotope Effects in C-H Bond Functionalizations by Transition-Metal Complexes, *Angew. Chem. Int. Ed.* **2012**, *51*, 3066-3072.
(63) Fristrup, P.; Kreis, M.; Palmelund, A.; Norrby, P. O.; Madsen, R. The Mechanism for the Rhodium-Catalyzed Decarbonylation of Aldehydes: A Combined Experimental and Theoretical Study, *J. Am. Chem. Soc.* **2008**, *130*, 5206-5215.
(64) Ghosh, R.; Zhang, X. W.; Achord, P.; Emge, T. J.; Krogh-Jespersen, K.; Goldman, A. S. Dimerization of Alkynes Promoted by a Pincer-Ligated Iridium Complex. C-C Reductive Elimination Inhibited by Steric Crowding, *J. Am. Chem. Soc.* **2007**, *129*, 853-866.
(65) Zuidema, E.; Escorihuela, L.; Eichelsheim, T.; Carbo, J. J.; Bo, C.; Kamer, P. C. J.; Van Leeuwen, P. W. N. M. The Rate-Determining Step in the Rhodium-Xantphos-Catalysed Hydroformylation of 1-Octene, *Chem. Eur. J.* **2008**, *14*, 1843-1853.
(66) Arndt, M.; Salih, K. S. M.; Fromm, A.; Goossen, L. J.; Menges, F.; Niedner-Schatteburg, G. Mechanistic Investigation of the Ru-Catalyzed Hydroamidation of Terminal Alkynes, *J. Am. Chem. Soc.* **2011**, *133*, 7428-7449.
(67) Steffen, A.; Ward, R. M.; Tay, M. G.; Edkins, R. M.; Seeler, F.; van Leeuwen, M.; Palsson, L. O.; Beeby, A.; Batsanov, A. S.; Howard, J. A. K.; Marder, T. B. Regiospecific Formation and Unusual Optical Properties of 2,5-

Bis(arylethynyl)rhodacyclopentadienes: A New Class of Luminescent Organometallics, *Chem. Eur. J.* **2014**, *20*, 3652-3666.

(68) Ma, W. Y.; Yu, C.; Chen, T. Y.; Xu, L.; Zhang, W. X.; Xi, Z. F. Metallacyclopentadienes: synthesis, structure and reactivity, *Chem. Soc. Rev.* **2017**, *46*, 1160-1192.

(69) Krossing, I. The Facile preparation of Weakly Coordinating Anions: Structure and Characterisation of Silverpolyfluoroalkoxyaluminates $AgAl(OR_F)_4$, calculation of the Alkoxide Ion Affinity, *Chem. Eur. J.* **2001**, *7*, 490-502.

(70) Addition of 1 equivalent of PPh_3 to **13** displaced the pyran with the formation of the Rh(I)-complex, [Rh(*mer*-κ^3-P,O,P-DPEPhos)(PPh_3)][BAr^F_4]. The unbound pyran was characterized by NMR spectroscopy and ESI-MS, data for which correspond well with previously reported α-pyrans with related structures, See Supporting Materials and (a) Buchi, G.; Yang, N. C. Light-Catalyzed Organic Reactions. VI. The Isomerization of Some Dienones. *J. Am. Chem. Soc.* **1957**, *79*, 2318-2323; (b) Gosink, T. A. Valence Isomers. Substituent Effects on the Equilibrium between 2H-Pyrans and Cis Dienones. *J. Org. Chem.* **1974**, *39*, 1942-1944; (c) Marvell, E. N.; Gosink, T. Valence Isomerization of 2,4,6-Trimethyl-2H-Pyran. *J. Org. Chem*. **1972**, *37*, 3036-3037; (d) Marvell, E. N.; Gosink, T.; Caple, G.; Chadwick, T.; Zimmer, G. Rates of Electrocyclic Reactions - Conversion of α-Pyrans to Cis Dienones. *J. Org. Chem.* **1972**, *37*, 2992-2997.

(71) Hansson, S.; Miller, J. F.; Liebeskind, L. S. Synthesis and Reactions of Enantiomerically Pure Molybdenum π-Complexes of 2*H*-Pyran. A General Approach to the Enantiospecific Synthesis of *cis*-2,5-Disubstituted 5,6-Dihydro-2*H*-pyrans and *cis*-2,6-Disubstituted Tetrahydropyrans, *J. Am. Chem. Soc.* **1990**, *112*, 9660-9661.

(72) Tsuchikama, K.; Yoshinami, Y.; Shibata, T. Rhodium-Complex-Catalyzed [2 + 2 + 2] Cycloaddition of Diynes and Carbonyl Compounds, *Synlett* **2007**, 1395-1398.

(73) Tanaka, K.; Otake, Y.; Sagae, H.; Noguchi, K.; Hirano, M. Highly Regio-, Diastereo-, and Enantioselective [2+2+2] Cycloaddition of 1,6-Enynes with Electron-Deficient Ketones Catalyzed by a Cationic Rh^I/H_8-binap complex, *Angew. Chem. Int. Ed.* **2008**, *47*, 1312-1316.

(74) Tekavec, T. N.; Louie, J. Nickel-Catalyzed Cycloadditions of Unsaturated Hydrocarbons, Aldehydes, and Ketones, *J. Org. Chem.* **2008**, *73*, 2641-2648.

(75) Miyauchi, Y.; Kobayashi, M.; Tanaka, K. Rhodium-Catalyzed Intermolecular [2+2+2] Cross-Trimerization of Aryl Ethynyl Ethers and Carbonyl Compounds To Produce Dienyl Esters, *Angew. Chem. Int. Ed.* **2011**, *50*, 10922-10926.

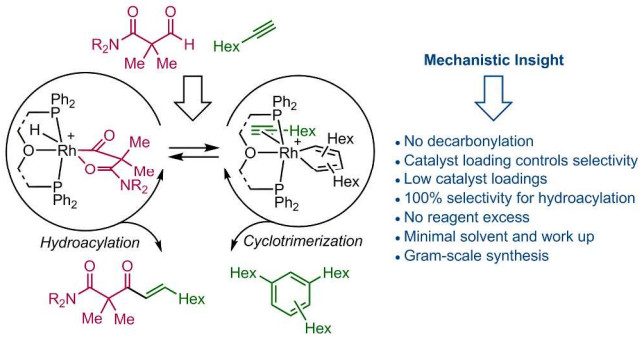

For Table of Contents

(76) Hooper, J. F.; Chaplin, A. B.; Gonzalez-Rodriguez, C.; Thompson, A. L.; Weller, A. S.; Willis, M. C. Aryl Methyl Sulfides as Substrates for Rhodium-Catalyzed Alkyne Carbothiolation: Arene Functionalization with Activating Group Recycling, *J. Am. Chem. Soc.* **2012**, *134*, 2906-2909.

(77) Preliminary studies show that addition of trihexyl benzenes **8a**/**8b** to bis-acetone **1**, results in an equilibrium mixture of 1:14 that strongly favours the bis-acetone complex **1**.

(78) Pike, S. D.; Pernik, I.; Theron, R.; McIndoe, J. S.; Weller, A. S. Relative binding affinities of fluorobenzene ligands in cationic rhodium bisphosphine η^6-fluorobenzene complexes probed using collision-induced dissociation, *J. Organomet. Chem.* **2015**, *784*, 75-83.

(79) Arene ligands are historically considered to be poisons in catalysis with Rh(I); see Heller, D.; Drexler, H. J.; Spannenberg, A.; Heller, B.; You, J. S.; Baumann, W. The Inhibiting Influence of Aromatic Solvents on the Activity of Asymmetric Hydrogenations. *Angew. Chem. Int. Ed.* **2002**, *41*, 777-780; Meissner, A.; Alberico, E.; Drexler, H. J.; Baumann, W.; Heller, D. Rhodium diphosphine complexes: a case study for catalyst activation and deactivation. *Catal. Sci. Technol.* **2014**, *4*, 3409-3425.

(80) Mcalister, D. R.; Bercaw, J. E.; Bergman, R. G. Parallel Reaction Pathways in Cobalt-Catalyzed Cyclotrimerization of Acetylenes, *J. Am. Chem. Soc.* **1977**, *99*, 1666-1668.

(81) Agenet, N.; Gandon, V.; Vollhardt, K. P. C.; Malacria, M.; Aubert, C. Cobalt-Catalyzed Cyclotrimerization of Alkynes: The Answer to the Puzzle of Parallel Reaction Pathways, *J. Am. Chem. Soc.* **2007**, *129*, 8860-8871.

(82) Monillas, W. H.; Young, J. F.; Yap, G. P. A.; Theopold, K. H. A well-defined model system for the chromium catalyzed selective oligomerization of ethylene, *Dalton. Trans.* **2013**, *42*, 9198-9210.

(83) Yamamoto, K.; Nagae, H.; Tsurugi, H.; Mashima, K. Mechanistic understanding of alkyne cyclotrimerization on mononuclear and dinuclear scaffolds: [4+2] cycloaddition of the third alkyne onto metallacyclopentadienes and dimetallacyclopentadienes, *Dalton. Trans.* **2016**, *45*, 17072-17081.

(84) Jimenez-Gonzalez, C.; Ponder, C. S.; Broxterman, Q. B.; Manley, J. B. Using the Right Green Yardstick: Why Process Mass intensity Is Used in the Pharmaceutical Industry To Drive More Sustainable Processes, *Org. Process Res. Dev.* **2011**, *15*, 912-917.

(85) Sholl, D. S.; Lively, R. P. Seven chemical separations to change the world, *Nature* **2016**, *532*, 435-437.

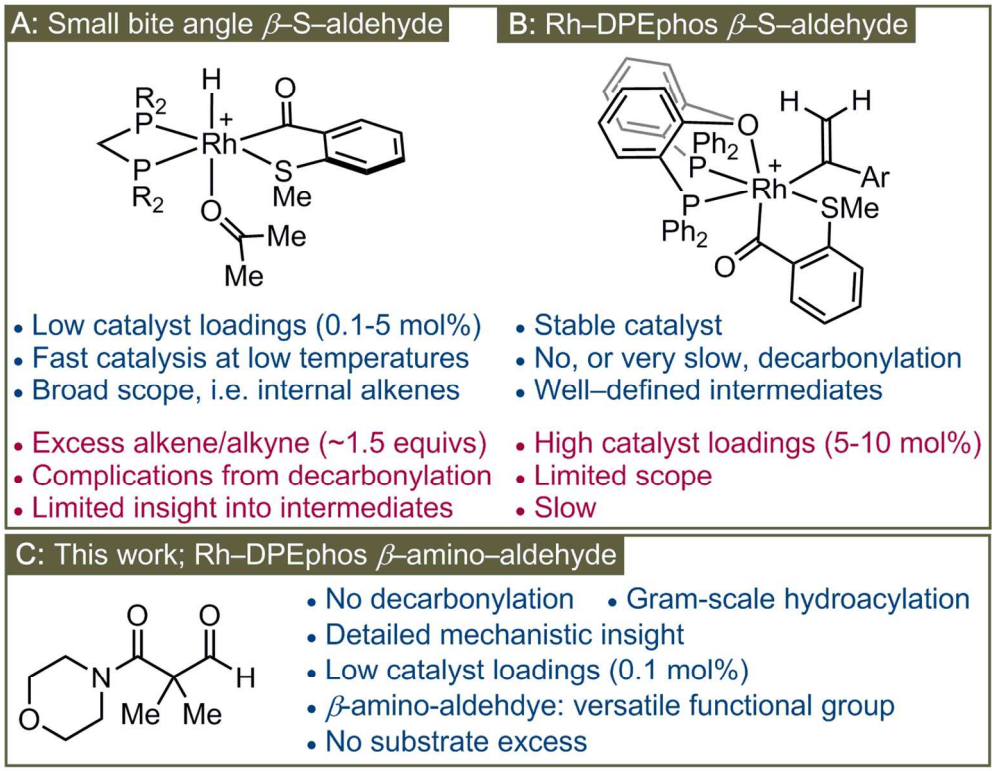

122x94mm (300 x 300 DPI)

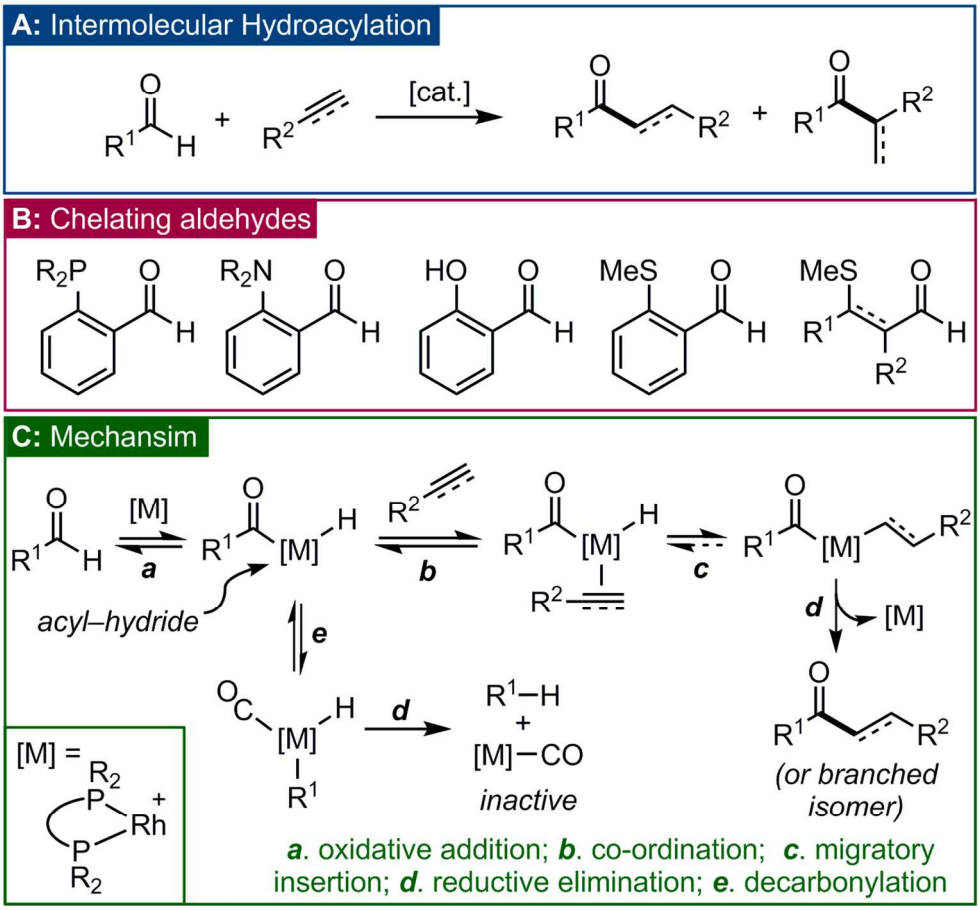

122x113mm (300 x 300 DPI)

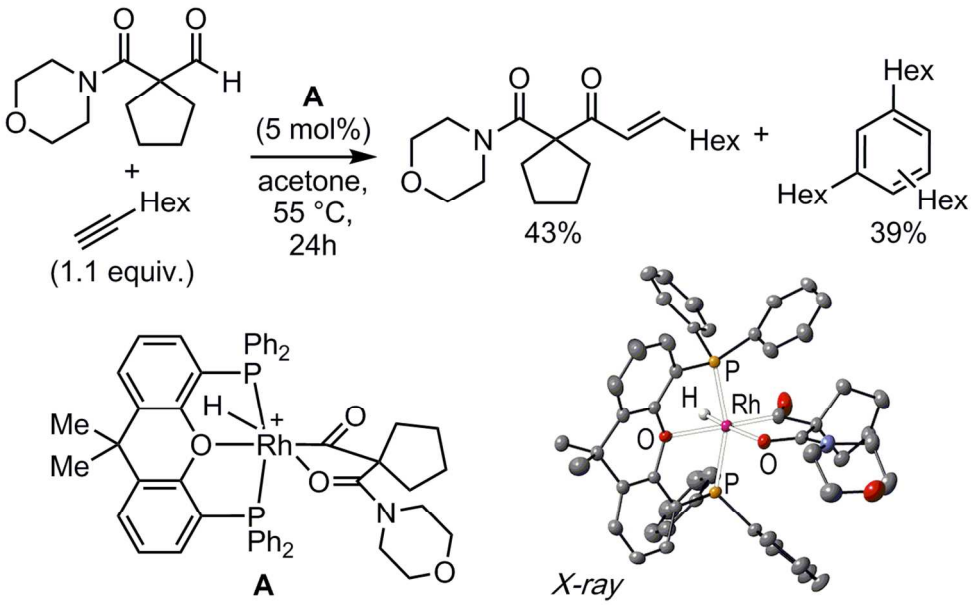

122x76mm (300 x 300 DPI)

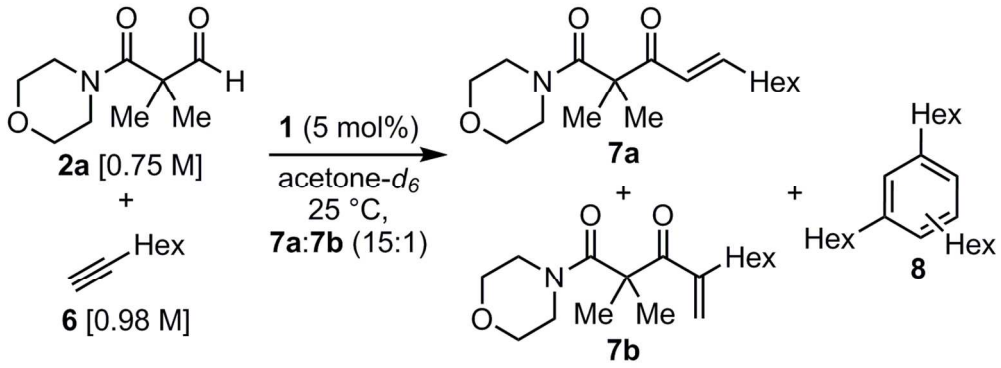

121x45mm (300 x 300 DPI)

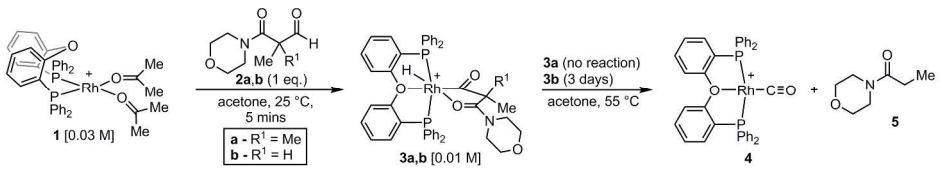

255x43mm (300 x 300 DPI)

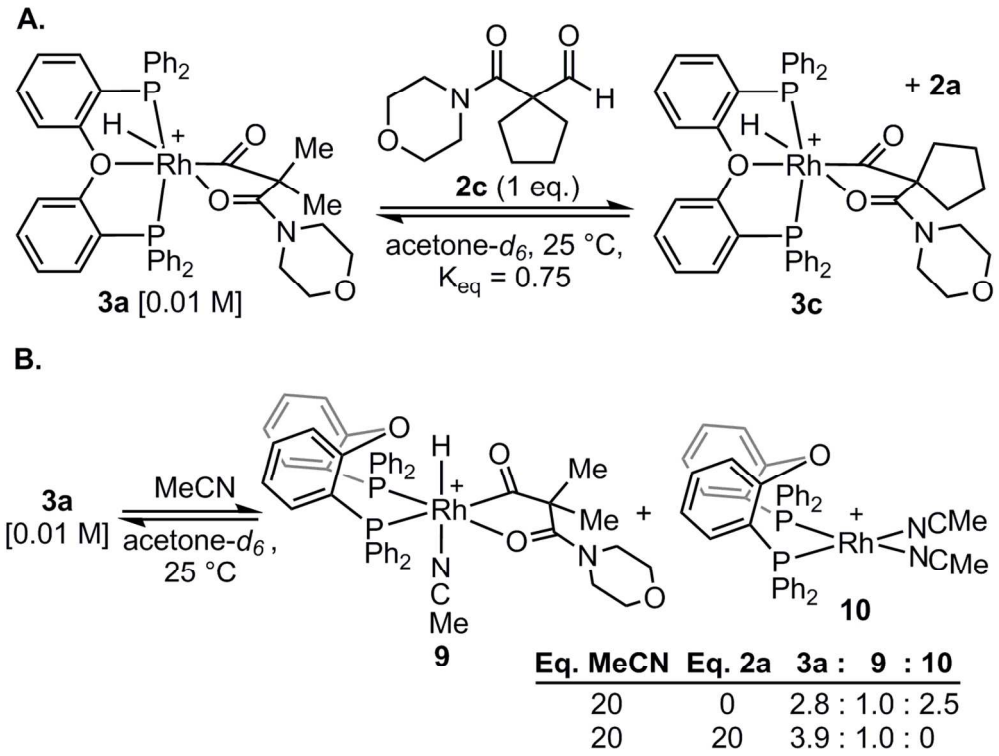

121x93mm (300 x 300 DPI)

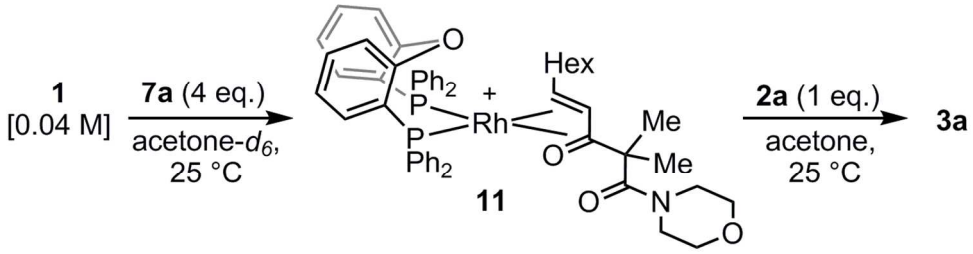

122x33mm (300 x 300 DPI)

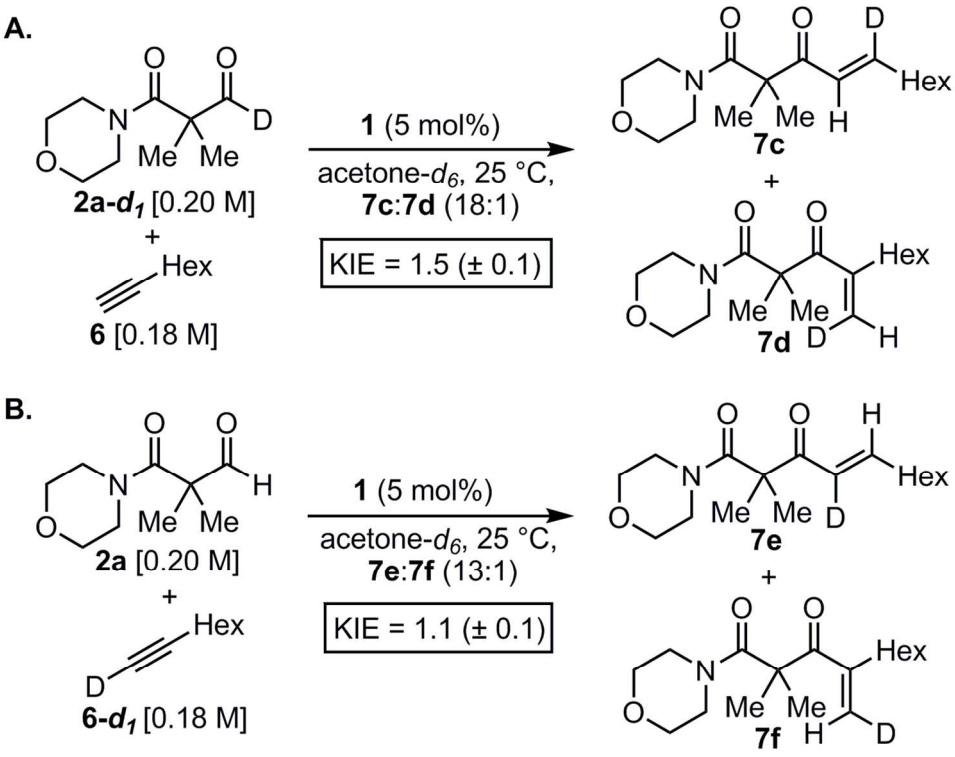

122x94mm (300 x 300 DPI)

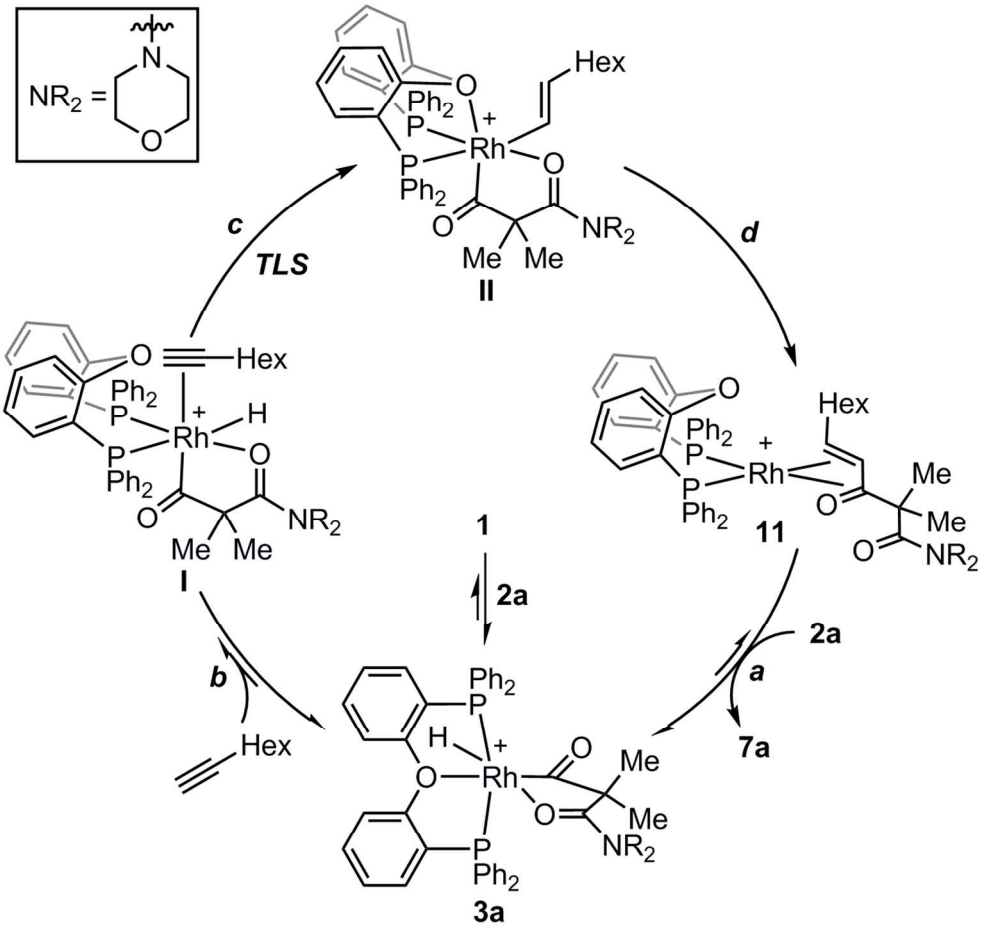

121x113mm (300 x 300 DPI)

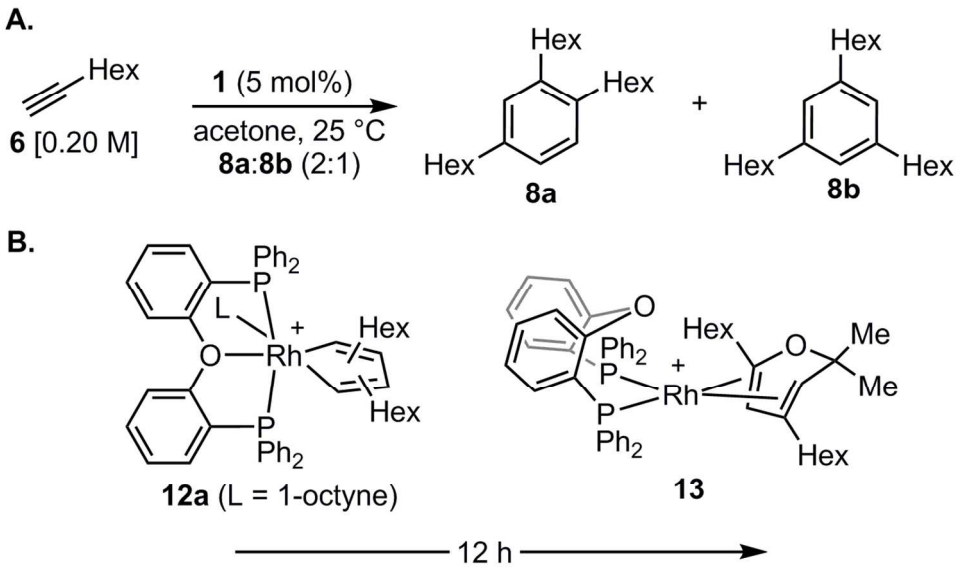

121x71mm (300 x 300 DPI)

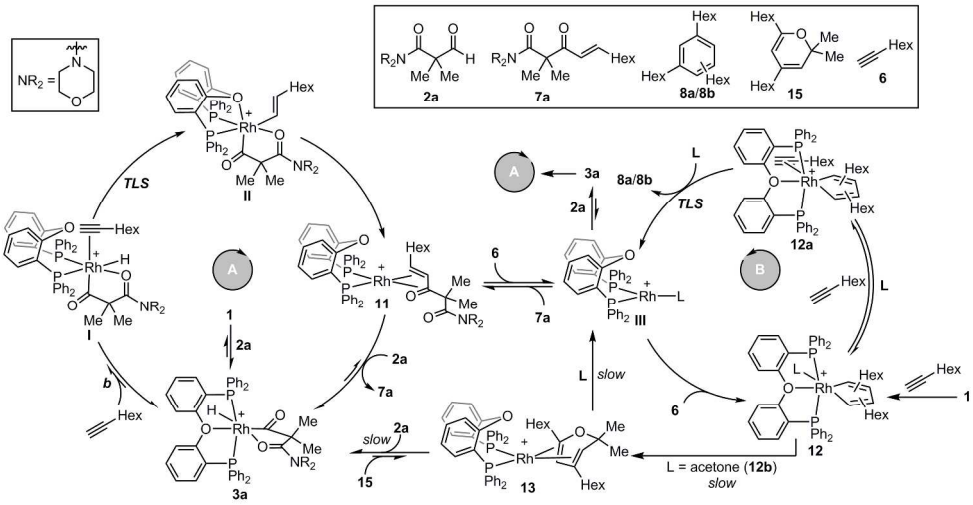

254x128mm (300 x 300 DPI)

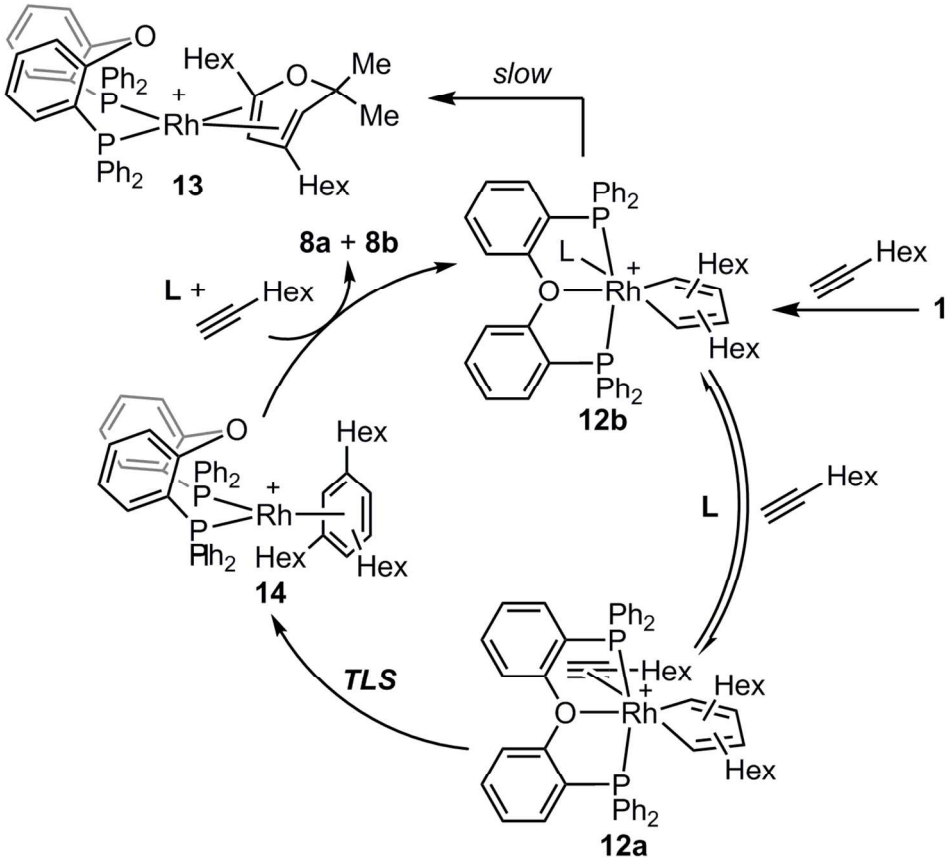

121x105mm (300 x 300 DPI)

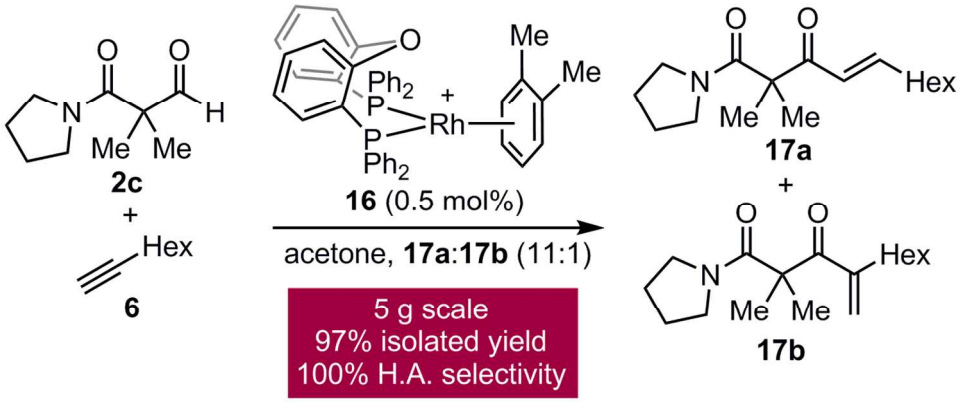

122x50mm (300 x 300 DPI)

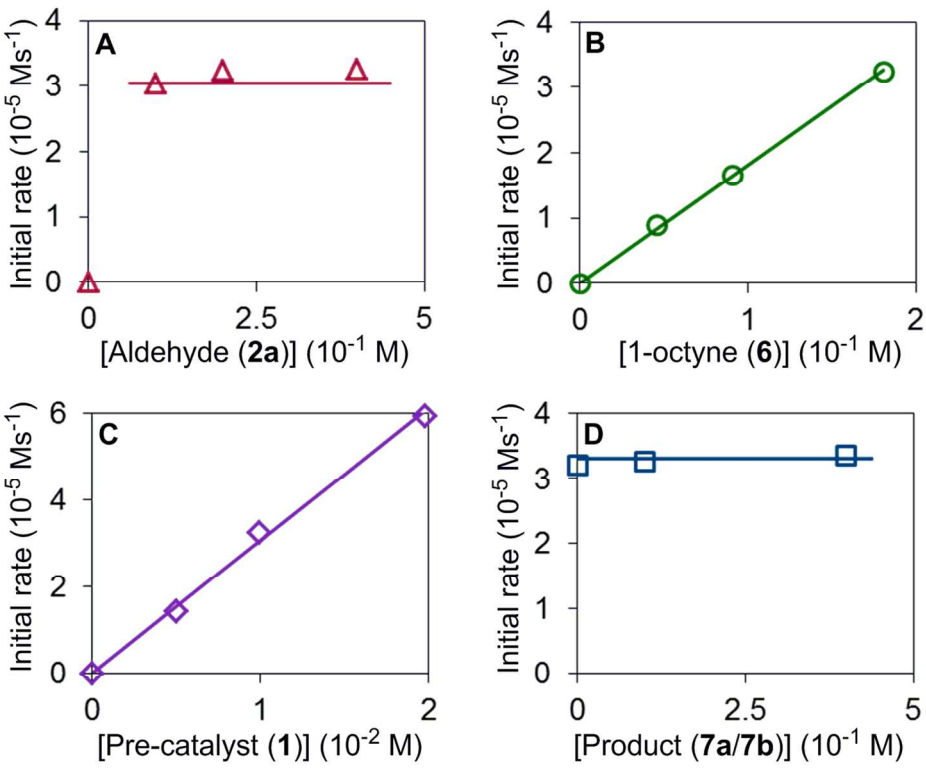

121x96mm (300 x 300 DPI)

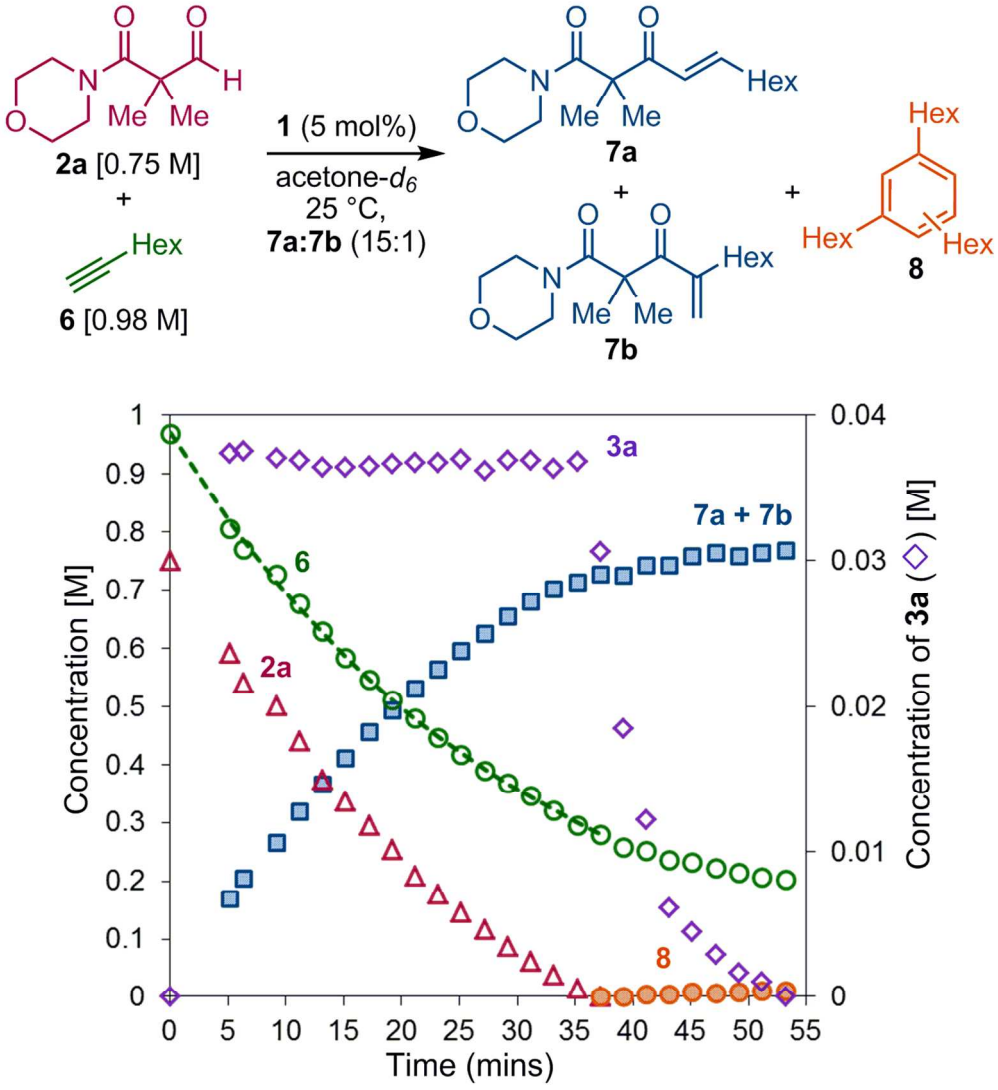

121x133mm (300 x 300 DPI)

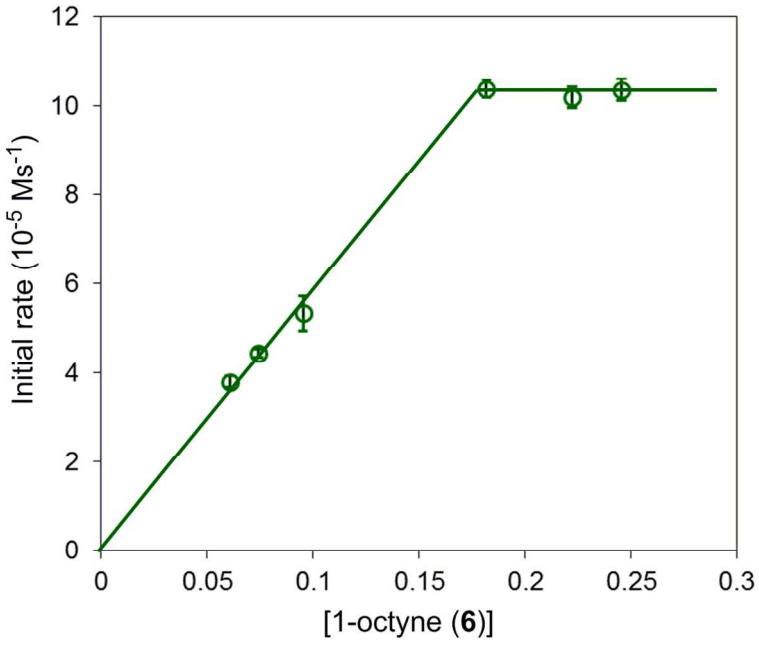

121x80mm (300 x 300 DPI)

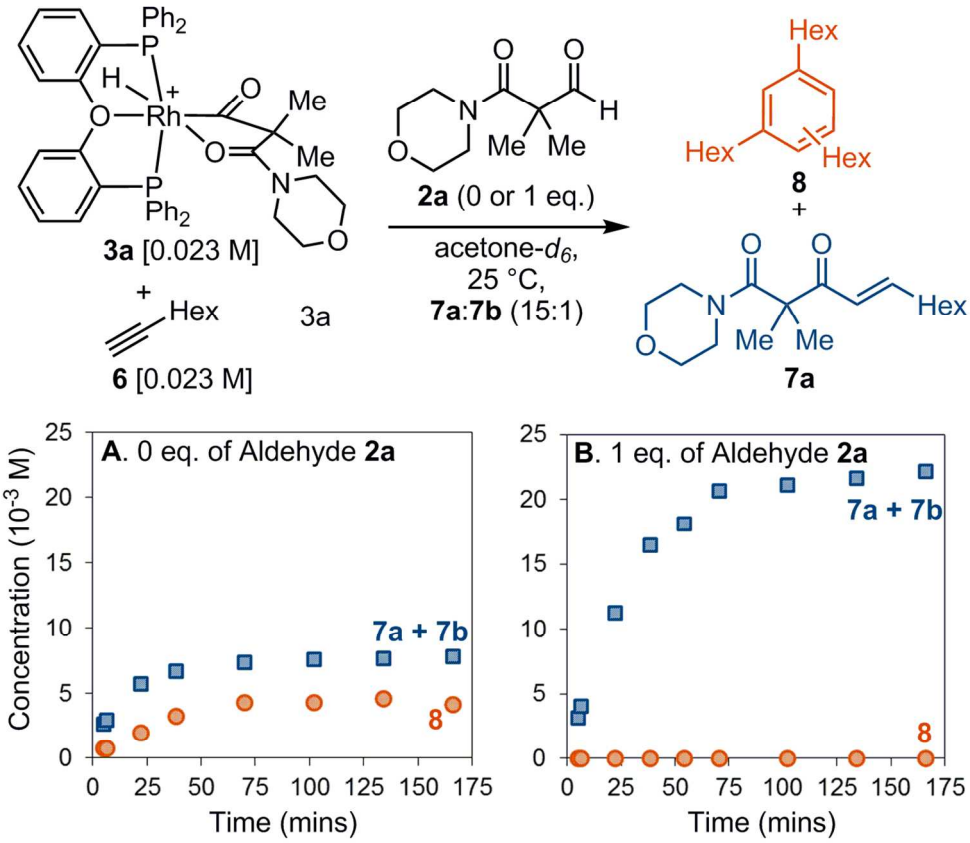

125x106mm (300 x 300 DPI)

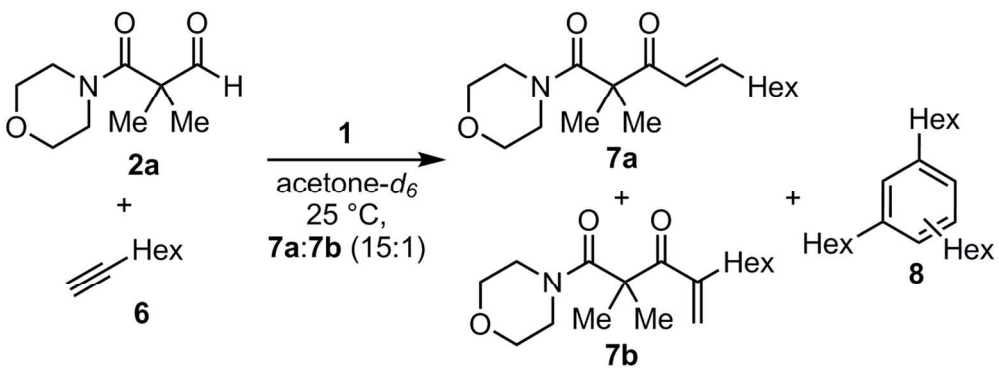

121x45mm (300 x 300 DPI)

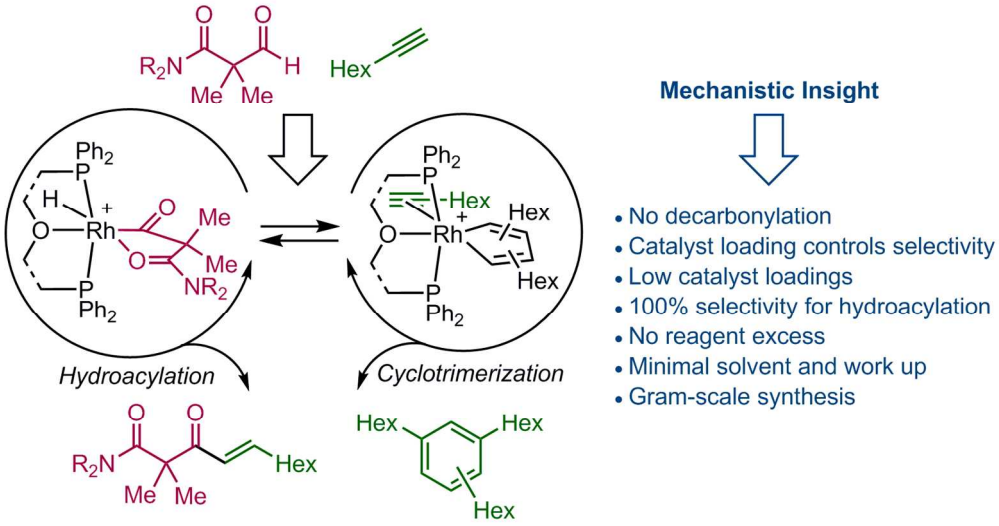

149x78mm (300 x 300 DPI)